The American Journal of Pathology, Vol. 184, No. 3, March 2014

ELSEVIER

The American Journal of
PATHOLOGY

ajp.amjpathol.org

CELL INJURY, REPAIR, AGING, AND APOPTOSIS

Depletion of Apoptosis Signal-Regulating Kinase 1 Prevents Bile Duct Ligation—Induced Necroinflammation and Subsequent Peribiliary Fibrosis

Hirotsugu Noguchi,* Sohsuke Yamada,* Atsunori Nabeshima,* Xin Guo,* Akihide Tanimoto,† Ke-Yong Wang,*‡ Shohei Kitada,*§ Takashi Tasaki,* Tatsuo Takama,*¶ Shohei Shimajiri,* Hasita Horlad,‖ Yoshihiro Komohara,‖ Hiroto Izumi,** Kimitoshi Kohno,†† Hidenori Ichijo,‡‡ and Yasuyuki Sasaguri*

From the Departments of Pathology and Cell Biology, School of Medicine, University of Occupational and Environmental Health, Kitakyushu; the Department of Molecular and Cellular Pathology,† Kagoshima University Graduate School of Medical and Dental Sciences, Kitakyushu; the Bio-information Research Center,‡ and the Departments of Urology,§ Emergency Medicine,¶ Occupational Pneumology,** and Molecular Biology,†† School of Medicine, University of Occupational and Environmental Health, and the Department of Cell Pathology,‖ Faculty of Medical and Pharmaceutical Sciences, Graduate School of Medical Sciences, Kumamoto University, Kitakyushu; and the Laboratory of Cell Signaling,‡‡ Graduate School of Pharmaceutical Sciences, The University of Tokyo, and Core Research for Evolutional Science and Technology, Tokyo, Japan*

Accepted for publication November 26, 2013.

Address correspondence to Sohsuke Yamada, M.D., Ph.D., Department of Pathology and Cell Biology, School of Medicine, University of Occupational and Environmental Health, 1-1 Iseigaoka, Yahatanishi-ku, Kitakyushu 807-8555, Japan. E-mail: sousuke@med.uoeh-u.ac.jp.

Apoptosis signal-regulating kinase 1 (ASK1), also known as mitogen-activated protein kinase kinase kinase (MAP3K), is ubiquitously expressed and situated in an important upstream position of many signal transduction pathways. ASK1 plays a pivotal role in stressor-induced cell survival and inflammatory reactions. To ascertain the regulatory functions of ASK1 in bile duct ligation (BDL)—induced liver injury, we examined the net effects of ASK1 depletion on hepatic necroinflammation and/or fibrosis. We subjected C57BL/6 wild-type (WT) or *ASK1*-deficient (*ASK1*$^{-/-}$) mice to sham or BDL surgery for 14 days. In day 3 BDL animals, *ASK1*$^{-/-}$ mice had significantly fewer bile infarcts along with more reduced interlobular or portal inflammatory infiltrate of various immune cells, including neutrophils, compared with WT mice in which ASK1 expression was markedly activated. Morphologically apoptotic hepatocytes or cholangiocytes were negligible in both the sham and BDL animals. In contrast, *ASK1*$^{-/-}$ mice had significantly less proliferating activity of not only hepatocytes but also large cholangiocytes than WT mice. Day 14 BDL *ASK1*$^{-/-}$ mice manifested potential antifibrogenic aspects of *ASK1* deficiency, characterized by significantly fewer activated peribiliary fibrogenic cells and peribiliary fibrosis. These observations indicate that ASK1-mediated hepatic necroinflammation and proliferation, but not apoptosis, are closely linked to liver fibrosis and fibrogenesis. A specific ASK1 pathway blocker or inhibitor might offer a therapeutic strategy against human cholestatic diseases. *(Am J Pathol 2014, 184: 644—661; http://dx.doi.org/10.1016/j.ajpath.2013.11.030)*

It was previously proposed that hepatocytes undergoing apoptosis might provide a critical hit to drive progression from chronic inflammation to cirrhosis, especially in cholestatic injury, such as primary biliary cirrhosis, primary sclerosing cholangitis, biliary atresia, or chronic cholelithiasis, with reference to a single laboratory.[1—4] In striking contrast, several other groups[5—9] have recently suggested that there is no evidence of hepatocellular apoptosis using morphologic criteria, but not terminal deoxynucleotidyl transferase end-labeling (TUNEL) staining, in or around necrotic foci (ie, bile infarcts) after bile duct ligation (BDL), which is used to induce cholestasis in rodents.[1—3,5—9] They also concluded that BDL-induced oncotic necrosis but not apoptosis of hepatocytes is closely correlated with the severity of the inflammatory response, including high chemokine and/or cytokine expression.[6,8,9] Meanwhile, although cholangiocytes are a minor component of liver cells, comprising merely 3% to 4% of the rodent liver, cells lining the large bile ducts (large cholangiocytes) are the

This work was supported in part by Grants-in-Aid for Scientific Research (19590413, 20590416, and 24790394) from the Ministry of Education, Culture, Sports, Science and Technology, Tokyo, Japan (S.Y., A.T., and Y.S.).

H.N. and S.Y. contributed equally to this work.

Disclosures: None declared.

http://dx.doi.org/10.1016/j.ajpath.2013.11.030

main target in animal models of cholestasis and intractable human cholestatic diseases.[10,11] Previous studies revealed that rodent cholangiocytes are mitotically dormant under basal conditions, whereas large but not small cholangiocytes undergo significant proliferation, leading to subsequent liver fibrosis after BDL injury, even though morphologic or functional heterogeneity is noted in large versus small cholangiocytes.[12–14] Nevertheless, the regulation of biliary injury and proliferation during cholestasis is multifactorial and complex, and the various roles of large cholangiocytes in the initiation and progression of cholestatic liver diseases are still debatable.[12,14] Hence, key factors and signaling pathways that control the responses to injury in not only hepatocytes but also cholangiocytes need to be identified.

Apoptosis signal-regulating kinase 1 (ASK1) is a mitogen-activated protein kinase kinase kinase (MAP3K) family member that is activated through distinct mechanisms in response to various cytotoxic stressors, including oxidative stress mediated by hydrogen peroxide, endoplasmic reticulum (ER) stress, and immune system mediators, such as tumor necrosis factor (TNF)-α, IL-1β, or Fas ligands.[15,16] ASK1 is situated in an important upstream position for many signal transduction pathways, such as the c-Jun N-terminal kinase (JNK) and p38 MAP kinase (MAPK), which subsequently induce inflammation and intrinsic apoptotic signaling through mitochondria-dependent caspase activation.[15–17] Previous reports using *ASK1*$^{-/-}$ mice or *ASK1* overexpressing transgenic mice confirmed that ASK1 plays a pivotal role in the regulation of cardiomyocyte apoptosis in ischemia-reperfusion injury models.[18,19] Moreover, we recently found that activation of ASK1 signaling enhances hyperlipidemia-induced necrotic lipid core formation by inducing macrophage apoptosis and accelerates mechanical injury–induced vascular remodeling via increased neovascularization and proinflammatory reaction and by stimulating apoptosis of smooth muscle cells and/or endothelial cells.[17,20] ASK1 plays a significant role in the regulation of vascular cell apoptosis and inflammatory signaling *in vivo* and is correlated with plaque vulnerability in atherosclerosis.[20] Other studies report that ASK1 expression plays a critical role *in vivo* in the regulation of apoptosis in type 2 pneumocytes in lung injury, with both antiapoptotic and anti-inflammatory properties.[21] However, few studies have investigated the relationship between ASK1 signaling pathway and cholestasis-induced injury, even though ASK1 is ubiquitously expressed.

In the current study, we examined the roles of ASK1 in BDL-induced cholestatic liver injury using mice genetically deficient for *ASK1* (*ASK1*$^{-/-}$). Furthermore, we aimed to determine the net effects and key factors of ASK1 in liver necroinflammation or subsequent fibrosis.

Materials and Methods

Animals and BDL Model

Experiments were performed using 6- to 8-week-old, male, C57BL/6 wild-type (WT) and *ASK1*$^{-/-}$ mice,[17,20] weighing 18 to 22 g, maintained in a temperature and light-controlled facility with free access to standard rodent chow diet and water. *ASK1*$^{-/-}$ mice were developed on a C57BL/6 background.[17,20] To produce a ligation-induced cholestatic liver injury (BDL) model, the peritoneal cavity was opened after a midline upper-abdominal incision, and the common bile duct was double-ligated with sterile surgical 7-0 silk sutures (Alfresa Pharma Corp., Tokyo, Japan) and cut between the ligatures in two groups of mice at 6 to 8 weeks of age under anesthesia [intraperitoneal injection of ketamine (100 mg/kg) (Daiichi Sankyo Co., Tokyo, Japan) and medetamidine (2 mg/kg) (Meiji Yakuhin Co., Tokyo, Japan)], as previously described.[20] Sham-operated mice, as controls, underwent laparotomy with exposure but no ligation of the common bile duct. The fascia and skin of the midline abdominal incision were closed with sterile surgical 6-0 silk sutures (Alfresa Pharma Corp.). After a defined period of BDL or sham operation at 3 or 14 days, animals were euthanized by exsanguination under reanesthetization with an i.p. injection of ketamine-medetamidine, as follows: the peritoneal cavity was reopened, and blood samples were taken from the inferior vena cava, followed by immediate cannulation of the suprahepatic vena cava. In all animals, after blood was flushed out of the liver via the suprahepatic vena cava catheter, livers were excised and cut into small pieces and used for various experiments as described below. The 24-hour urine of day 3 BDL mice was collected using mouse metabolic cages (Sugiyama-Gen Co., Ltd., Tokyo, Japan).

The Ethics Committee of Animal Care and Experimentation, University of Occupational and Environmental Health (Japan), approved the protocols. They were performed according to the Institutional Guidelines for Animal Experiments and the Law (no. 105) and Notification (no. 6) of the Japanese government. The investigation conformed to the *Guide for the Care and Use of Laboratory Animals* published by the US National Institutes of Health.

Histopathology

Liver specimens were stained with H&E, Masson's trichrome, or picrosirius red stain, or immunohistochemistry (IHC) preparations in sequential sections, after fixation in 10% neutral buffered formalin for 24 hours.[17,20,22–25] Analyses were performed in BDL-induced cholestatic livers in all experiments, whereas the sham-operated livers served as controls.

Livers embedded in paraffin for histologic examination were cut systematically in sequential sections of 4-μm thickness using a sliding microtome (Leica SM2010R; Leica Microsystems, Wetzler, Germany). For histologic analyses of the liver, images of H&E and special stained sections or IHC sections were captured and quantified using NanoZoomer Digital Pathology Virtual Slide Viewer software version 2.0 (Hamamatsu Photonics Corp., Hamamatsu, Japan). H&E-stained liver sections were used to measure the areas of bile infarcts (hepatic necrosis) and calculate the

percentage of necrotic area divided by total area. In addition, apoptotic cells were identified in 10 randomly selected fields of interlobular and portal tracts per these H&E sections (original magnification, ×400), using morphologic criteria (cell shrinkage, chromatin condensation and margination, and apoptotic bodies).[5–9] Liver fibrosis was quantified by Masson's trichrome and picrosirius red staining (Picrosirius Red Stain Kit; Polysciences, Inc., Warrington, PA) in 10 randomly selected fields of portal and periportal tracts per section (original magnification, ×400). In periportal tracts, fibers stained red with yellow birefringence under polarized light were defined as expressing collagen type I.[25] The proportions of collagen content were calculated for individual images in cholestatic BDL livers, excluding large bile ducts (>15-μm diameter) and vessels.

Analyses of Hepatic Cholestasis (BDL)—Induced Injury

Serum levels of total bilirubin and hepatic injury—related enzymes, including aspartate aminotransferase (AST), alanine aminotransferase (ALT), alkaline phosphatase, and total bile acids, were measured using commercial assay kits (Wako Pure Chemical Co., Osaka, Japan). To examine the hepatic bile acids, snap frozen liver tissue (30 mg) was homogenized and extracted with chloroform-methanol (2/1 v/v) solution. The organic phase was dried and resolubilized in 2-propanol. Then the hepatic contents of bile acids were determined using commercial assay kits (Wako Pure Chemical Co.). Urinary bilirubin concentrations were normalized with creatinine levels.

IHC and Double-Immunofluorescence Staining

One representative sequential section per mouse was prepared for IHC staining and was captured and evaluated by a NanoZoomer Digital Pathology Virtual Slide Viewer (Hamamatsu Photonics Corp.) to avoid potential bias.[17,20,23–25] Liver sections were stained with a goat polyclonal anti-mouse cytokeratin 19 (CK19) antibody (1:50; Santa Cruz Biotechnology, Santa Cruz, CA) to highlight the lining of small and large bile ducts (small and large cholangiocytes, respectively). For various analyses, the bile ducts were separated according to size (small, <15-μm diameter; large, >15-μm diameter).[12,14] We excluded tangentially sectioned bile ducts, where one cross-sectional diameter was three times larger than another diameter, from all analyses.[12,14] The hyperplastic and proliferating bile ductules were identified in the interface areas of portal tracts per section. In addition, intrahepatic bile duct mass (IBDM) was measured as followed: area occupied by $CK19^+$ bile ducts/total area × 100.[26]

To evaluate the severity of BDL-induced cholestasis on day 3, we determined the intensity of inflammation using a polyclonal rabbit anti-human CD3 antibody (1:1; Dako Cytomation Co., Tokyo, Japan), a rat anti-mouse Mac-2 monoclonal antibody (1:500; Cedarlane Laboratories Ltd., Burlington,

Table 1 Primers Used for Real-Time PCR and RT-PCR

Gene	Primer
Real-time PCR primers	
ASK1	
Forward	5′-ACGACCACCTCAGGGTCATTC-3′
Reverse	5′-TGGTCAGTTTCACAAAGTGTTTATATATCAG-3′
Probe	5′-AGACTGAAGACACCAGCGTGGTACCTCAAGT-3′
Caspase-3	
Forward	5′-AAGCCGAAACTCTTCATCATTCAG-3′
Reverse	5′-AGCCTCCACCGGTATCTTCTG-3′
Probe	5′-TGGACTGTGGCATTGAGACAGACAGTGG-3′
Bak	
Forward	5′-CTGGAACCCAACAGCATCTTG-3′
Reverse	5′-TGGTGAAGAGTTCGTAGGCATTC-3′
Probe	5′-CGGAGATGATATTAACCGGCGCTACGAC-3′
Bax	
Forward	5′-ATGGGCTGGACACTGGACTTC-3′
Reverse	5′-GAGGACTCCAGCCACAAAGATG-3′
Probe	5′-TGGCTGGGAAGGCCTCCTCTCCTACT-3′
IL-1β	
Forward	5′-TGCACTACAGGCTCCGAGATG-3′
Reverse	5′-GTACAAAGCTCATGGAGAATATCACTTG-3′
Probe	5′-TGTCGGACCCATATGAGCTGAAAGCTCTC-3′
IL-1R1	
Forward	5′-AGTTAAAAGCCAGTTTTATCGCTATCC-3′
Reverse	5′-CCCCCGATGAGGTAATTCTTG-3′
Probe	5′-AAATATTTTTGAGTCGGCGCATGTGCAGTTAAT-3′
IL-6	
Forward	5′-TTACACATGTTCTCTGGGAAATCG-3′
Reverse	5′-TTGGTAGCATCCATCATTTCTTTG-3′
Probe	5′-TGAGAAAAGAGTTGTGCAATGGCAATTCTGAT-3′
NF-κB	
Forward	5′-CTGACCCCTGTCCTCTCACATC-3′
Reverse	5′-CCGGTTTACTCGGCAGATCTT-3′
Probe	5′-TGATAACCGGGCCCCCAACACTG-3′
TNF-α	
Forward	5′-CCCAGACCCTCACACTCAGATC-3′
Reverse	5′-TGCTCCTCCACTTGGTGGTT-3′
Probe	5′-ATTCGAGTGACAAGCCTGTAGCCCACG-3′
TNFR2	
Forward	5′-TGGTCTGATTGTTGGAGTGACATC-3′
Reverse	5′-GGATTTCTCATCAGGCACATGAG-3′
Probe	5′-TGCATCATCCTGGTGCAGAGGAAAAAGA-3′
TLR4	
Forward	5′-CAGAACTTCAGTGGCTGGATTTATC-3′
Reverse	5′-TAGGGTTTCCTGTCAGTATCAAGTTTG-3′
Probe	5′-ACAAGGCATGGCATGGCTTACACCAC-3′
IFN-γ	
Forward	5′-CATTCATGAGTATTGCCAAGTTTGAG-3′
Reverse	5′-GCTTCCTGAGGCTGGATTCC-3′
Probe	5′-CCACAGGTCCAGCGCCAAGCATT-3′
iNOS	
Forward	5′-GCAGTGGAGAGATTTTGCATGAC-3′
Reverse	5′-ATGGACCCCAAGCAAGACTTG-3′
Probe	5′-CACCACAAGGCCACATCGGATTTCAC-3′
TGFβ-1	Mm00441724_m1 (Applied Biosystems Japan, Ltd., Tokyo, Japan).
PRDX1	
Forward	5′-TGTGGATTCTCACTTCTGTCATCTG-3′

(*table continues*)

Table 1 (*continued*)

Gene	Primer
Reverse	5′-GTGCGCTTGGGATCTGATATTAAG-3′
Probe	5′-CACACCCAAGAAACAAGGAGGATTGGGA-3′
PRDX2	
Forward	5′-CCCAGAATTACGGCGTGTTG-3′
Reverse	5′-CCCTTGGCATCGATGATAAAGA-3′
Probe	5′-AATGATGAGGGCATTGCTTACAGGG-3′
PRDX3	
Forward	5′-GGTGCTTTTCTTCTACCCTTTGG-3′
Reverse	5′-CACAGTTTACATCATGAAATTCATTGG-3′
Probe	5′-TTGTGTGTCCTACAGAAATTGTTGC-3′
PRDX4	
Forward	5′-TGGACGAGACACTGCGTTTG-3′
Reverse	5′-CTGGATCTGGGATTATTGTTTCACTAC-3′
Probe	5′-ACACTGACAAGCATGGAGAAGTCTGCCC-3′
PRDX5	
Forward	5′-GGAAGGCGACAGACTTATTATTGG-3′
Reverse	5′-CTCCACGTTCAGTGCCTTCAC-3′
Probe	5′-CGTCGGCTGAAAAGGTTCTCCATGGT-3′
PRDX6	
Forward	5′-GCCAAGAGGAATGTTAAGTTGATTG-3′
Reverse	5′-GTTTCACCATTGTAAGCATTGATGTC-3′
Probe	5′-CAATAGACAGTGTTGAGGATCATCATCTTGCCTGG-3′
CYP7A1	
Forward	5′-CGTGATCCTCTGGGCATCTC-3′
Reverse	5′-CTCTTGGCCAGCACTCTGTAATG-3′
Probe	5′-CAATGAAAGCAGCCTCTGAAGAAGTGAATGG-3′
Catalase	
Forward	5′-CCCTCCTCGTTCAGGATGTG-3′
Reverse	5′-TGATATCGTGGGTGACCTCAAAG-3′
Probe	5′-ACAGAGAGCGGATTCCTGAGAGAGTGGTACA-3′
SOD1	
Forward	5′-TGCAGGGAACCATCCACTTC-3′
Reverse	5′-CATGCTGGCCTTCAGTTAATCC-3′
Probe	5′-AAGCGGTGAACCAGTTGTGTTGTCAGGA-3′
SOD2	
Forward	5′-GCCTGCACTGAAGTTCAATGG-3′
Reverse	5′-ACCCAAAGTCACGCTTGATAGC-3′
Probe	5′-CTGGACAAACCTGAGCCCTAAGGGTGG-3′
FXR	
Forward	5′-CTGGAATATATGAACTCAGGCGTATG-3′
Reverse	5′-CCACAAACAACACACAGCTCATC-3′
Probe	5′-TAGCAGAGATGCCTGTAACAAAGAAGCCCC-3′
SHP	
Forward	5′-AAGGAGTATGCGTACCTGAAGG-3′
Reverse	5′-CTCCAAGACTTCACACAGTGC-3′
Probe	5′-CTCTTCAACCCAGATGTGCCAGGC-3′
VCAM-1	
Forward	5′-CTCATTCCCTGAAGATCCAGTAATTAA-3′
Reverse	5′-TCAAAGGGATACACATTAGGGACTGT-3′
Probe	5′-TGAGTGGGCCACTTGTGCATGGG-3′
ICAM-1	
Forward	5′-CAAACAGGAGATGAATGGTACATACG-3′
Reverse	5′-ACCAGAATGATTATAGTCCAGTTATTTTGAG-3′
Probe	5′-CCATGGGAATGTCACCAGGAATGTGTACC-3′
LFA-1	
Forward	5′-GGCCCCAGACTTTTGCTACTG-3′
Reverse	5′-GCAAGACCTGGTACCCAAAATG-3′

(*table continues*)

Table 1 (*continued*)

Gene	Primer
Probe	5′-CTACAACCTGGACACACGGCCTACGC-3′
VLA-4	
Forward	5′-CATCGTATATGAAATGAAAGGTAAAAAGC-3′
Reverse	5′-GATCTGAGAAGCCATCTGCATTG-3′
Probe	5′-GATCTGAGAAGCCATCTGCATTG-3′
PDGF-BB	
Forward	5′-AAGATCGAGATTGTGCGGAAGA-3′
Reverse	5′-AGCTGCCACTGTCTCACACTTG-3′
Probe	5′-AAGGCCACGGTGACGCTGGAAG-3′
PDGFRB	
Forward	5′-GCTCACGGTCTGAGCCATTC-3′
Reverse	5′-GACTCATAATCTTCAGCTCGGACATT-3′
Probe	5′-ATGCTGAAATCGACAGCCAGAAGTAGCGA-3′
18s rRNA	TaqMan Ribosomal RNA Control Reagents VIC Probe (Applied Biosystems, Foster City, CA; Cat. No. 4308329)
RT-PCR primers	
ASK1	
Forward	5′-GCCGTGCTGGACCGTTTTTAC-3′
Reverse	5′-GTGAGGCGTGATGTAAATAGGAAGC-3′
Neomycin	
Forward	5′-CTAAAGCGCATGCTCCAGACTGCCTTG-3′
Reverse	5′-GTGAGGCGTGATGTAAATAGGAAGC-3′
GAPDH	
Forward	5′-AATGCATCCTGCACCACCAACTGC-3′
Reverse	5′-GGAGGCCATGTAGGCCATGAGGTCC-3′

ON, Canada), or a rat anti-mouse Ly-6G antibody (Gr-1; 1:500; Birmingham, AL).[6,8,23–25,27] We counted the number of positive T lymphocytes, macrophages (Kupffer cells), and neutrophils in 10 randomly selected fields of portal and interlobular areas per section, respectively (original magnification, ×400).[25] In addition, the number of neutrophils present in the sinusoids and extravasated into the parenchymal tissue were counted in 10 randomly selected high-power fields of interlobular and portal areas of similar size per section, respectively (original magnification, ×400). The sum of sinusoidal and extravasated neutrophils was expressed as the total neutrophil sequestration in the liver.[28] Also, protein adducts of chlorotyrosine, as a useful marker of neutrophil-induced cytotoxicity, were detected by IHC using a rabbit antichlorotyrosine polyclonal antibody (1:50; Hycult Biotech, Uden, Netherlands).[28]

To assess the activation of peribiliary fibrogenic cells (ie, myofibroblasts) in BDL-injured portal tracts, we used a HistoMouse *Plus* Kit (Invitrogen Corp., Camarillo, CA) to block endogenous IgG and then stained tissues in mirror images of sequential sections with monoclonal mouse anti-human α-smooth muscle actin (α-SMA) (1:1000; Dako) and anti-human desmin (1:150; Dako) antibodies, as previously described.[29] The number of activated peribiliary fibrogenic cells (ie, myofibroblasts) was counted in 10 randomly selected fields of periportal or portal tracts per section, respectively (original magnification: ×400).[25,28]

For double-immunofluorescence, injured livers at day 14 BDL were labeled with mouse monoclonal α-SMA (1:1000; Dako) and goat polyclonal CK19 antibodies (1:50; Santa Cruz Biotechnology) and visualized with goat anti-mouse IgG antibodies conjugated with Alexa Fluor Dyes (red stained) and donkey anti-goat IgG antibodies conjugated with Alexa Fluor Dyes (green stained) (Invitrogen, Carlsbad, CA), respectively.[20,24] We applied the HistoMouse *Plus* Kit (Invitrogen) to block endogenous mouse IgG.[17,20,23–25]

To analyze the proliferative activity of bile ducts, Ki67 (MIB-1; 1:2000; Epitomics, Cambridge, UK) rabbit monoclonal antibody was applied. For double-immunofluorescence of proliferating cholangiocytes, injured livers of day 3 BDL mice were labeled with rabbit monoclonal Ki67 (1:2000; Epitomics) and goat polyclonal CK19 antibodies (1:50; Santa Cruz Biotechnology) and visualized with goat anti-rabbit IgG antibodies conjugated with Alexa fluor Dyes (green stained) and donkey anti-goat IgG antibodies conjugated with Alexa fluor Dyes (red stained) (Invitrogen), respectively.[20,24] More than 100 large or small cholangiocytes were counted in 10 randomly selected fields of portal or periportal tracts per section and viewed by confocal laser scanning microscopy (LSM5 Pascal Exciter; Carl Zeiss, Oberkochen, Germany) (original magnification, ×400).

To evaluate ASK1 expression in BDL-injured or sham-operated livers, we used mouse monoclonal antibody to phosphorylated ASK1 (p-ASK1; 1:200; Wako Pure Chemical Co.).[17,20]

For IHC or immunofluorescence studies, we examined one section from each of 5 or 10 mice per experimental group. All histologic and IHC slides were evaluated by two independent certified pathologists (Sohsuke Yamada and Shohei Shimajiri) who were masked to the physical outcome or other biological and pathological data for each sample. In case of disagreement, a consensus score was determined by a third board-certified pathologist (Yasuyuki Sasaguri). Agreement between observers was excellent (>0.9) for all sections investigated as measured by interclass correlation coefficient.

TUNEL and 5′-Bromo-2′-Deoxyuridine (BrdU) Staining

TUNEL assays were performed using an *In Situ* Cell Death Detection Kit (POD; Roche Applied Science, Mannheim, Germany).[17,20,23–25] In addition, BDL-injured livers on day 3 were labeled with antifluorescein antibodies (brown stained) (TUNEL POD; Roche Applied Science) or fluorescein-conjugated TUNEL reaction mixture (green stained) (Roche Applied Science) and goat polyclonal anti-CK19 antibody (1:50; Santa Cruz Biotechnology) and, for the latter, visualized with donkey anti-goat IgG antibodies conjugated with Alexa Fluor Dyes (red stained) (Invitrogen) by confocal laser scanning microscopy (LSM5 Pascal Exciter) (original magnification, ×400).[20,24] For quantitative analysis, we counted $TUNEL^+$ hepatocytes and cholangiocytes (brown stained) in 10 randomly selected fields around the bile infarcts per section (original magnification, ×400).[25]

To label proliferating large to small cholangiocytes in injured livers 3 days after BDL, BrdU (50 mg/kg body weight; Sigma, St. Louis, MO) was subcutaneously injected 2 hours before sacrifice. BrdU-incorporated cells were detected by IHC using a monoclonal mouse anti-BrdU antibody (Roche Applied Science, Lewes, UK).[17,20,24]

High-Performance Liquid Chromatography Analysis of Lipoprotein

Three days after BDL, the mice were fasted for 7 hours, and blood was collected from the inferior vena cava into a microtube that contained 5 μL of 0.5 mol/L EDTA. Samples were centrifuged for 12 minutes at 5500 × *g* at 4°C, and the resulting serum was stored at −80°C until assayed. Lipoproteins were analyzed by high-performance liquid chromatography using molecular sieve columns (Skylight Biotech Inc., Akita, Japan), as previously described.[17,24,25,30]

Measurement of Serum TBARS Levels

As a quantitative marker of oxidative stress closely associated with the development of cholestasis on day 3 after BDL surgery, we measured serum thiobarbituric acid reactive substance (TBARS) levels using a TBARS Assay Kit (Cayman Chemical Company, Ann Arbor, MI).[24,25] Results are expressed as nanomoles of malondialdehyde (MDA) per milligram of low-density lipoprotein (LDL) protein.

RT-PCR and Real-Time RT-PCR

Total RNAs were extracted with Trizol reagents (Invitrogen) from livers of mice sacrificed on day 3 or 14 after BDL injury, after careful removal of blood cells, using the sham-operated livers as controls. All procedures were performed as described previously.[17,20,22–25,30] RNase-free conditions were used to prevent mRNA degradation. First-strand cDNA was synthesized with Superscript II RT (Invitrogen) using random primers, according to the manufacturer's instructions. Quantitative real-time RT-PCR was performed using the TaqMan fluorogenic probe method with a LightCycler 480 System II PCR machine (Roche Diagnostics K.K., Tokyo, Japan). Sequences of specific primers for RT-PCR are summarized in Table 1. Cycling conditions were as follows: 50°C for 2 minutes and 95°C for 10 minutes followed by 45 cycles of 95°C for 15 seconds and 60°C for 1 minute. The C_T values were measured corresponding to the cycle number at which the fluorescent emission, monitored in real time, reached a threshold of 10 SDs above the mean baseline from cycles 1 to 15. Serial 1:10 dilutions of plasmid DNA that contained each target cDNA were analyzed and served as standard curves from which the rate of change of C_T values was determined. Copy numbers of target cDNA were estimated by standard curves.

All reactions for samples were performed in triplicate. Mean data were obtained from values of each reaction. To determine mRNA levels of various genes, an mRNA expression index was used where mRNA expression levels are standardized by 18s rRNA (Applied Biosystems, Foster City, CA). The mRNA expression index in arbitrary units (AU) was calculated as follows: mRNA expression index = (copy numbers of target gene mRNA/copy numbers of 18s rRNA) × 1 AU.

Microarray Studies and Data Analysis

DNA microarray analysis was performed using 3D-Gene software (Toray Industries, Kamakura, Kanagawa, Japan), as previously described.[31] High-quality RNA samples (1 μg each) prepared from injured livers of WT and *ASK1*$^{-/-}$ mice sacrificed on day 3 after BDL were amplified and labeled with cyanine 3 and cyanine 5 CTP (Amersham Biosciences Corp., Piscataway, NJ) to produce labeled cRNA using Agilent low-RNA-input fluorescent linear amplification kits following the manufacturer's protocol. After amplification and labeling, the dye-incorporation ratio was determined using a Nanodrop spectrophotometer, and ratios were within 10 to 20 pM per microgram of cRNA. For hybridization, 750 ng of cyanine 3− and 750 ng of cyanine 5−labeled cRNA was fragmented and hybridized to an Agilent Technologies Human 1A (V2) Gene Expression Microarray using the Agilent Gene Expression hybridization kit as described in the Two-Color Microarray-Based Gene Expression Analysis Version 4.0 manual. After hybridization, microarrays were washed and scanned with the Agilent dual-laser DNA microarray scanner. Scans were converted to data files with Agilent Feature Extraction software (version 8.5). Data were deposited in Gene Expression Omnibus (*http://www.ncbi.nlm.nih.gov/geo*; accession no. GSE23969) and analyzed with Microsoft Access version 2010 and Spotfire version 7.0 (Spotfire, Somerville, MA). Arrays were scanned by Agilent dual-laser DNA microarray scanner using SureScan technology, extracted by feature Extraction software version 7.1, and analyzed by Rosetta Resolver software version 3.2, build (3.2.2.0.33) (Rosetta Biosoftware, Kirkland, WA). Three replicate samples were used for each experiment. Genes were selected as significant using criteria of greater than twofold (up- or down-regulated) changes.

Preparation of Liver Hepatocytes and Analysis of ASK1 Expression

Liver hepatocytes were isolated from 8-week-old male *ASK1*$^{-/-}$ and WT mice fed a normal chow diet, as previously described.[25] All mice were anesthetized by i.p. injection of ketamine (Daiichi Sankyo Co.) and medetamidine (Meiji Yakuhin Co.). The abdominal cavity was opened, and the mesenteric and bilateral renal arteries were ligated. A ligature was placed around the portal vein at a site distal to the bifurcation and another around the inferior vena cava at a site proximal to the mesenteric artery. A tapered polyethylene cannula connected to a perfusion apparatus was inserted into the portal vein and was ligated in place. An 18-G needle was also inserted into the vena cava and ligated in place. Then liver perfusion medium (GIBCO17701-038; Gibco, Grand Island, NY) and collagenase type II solution medium (Gibco) with an oxygen and carbon dioxide mixture (95:5) at 37°C were injected into the cannula (4.5 mL/min). The collected cells were washed with Dulbecco's modified Eagle's medium; cultured in Dulbecco's modified Eagle's medium supplemented with 10% fetal bovine serum, 1% penicillin-streptomycin (Gibco), and 2 mmol/L glutamine (Gibco) at a density of 2 to 3 × 10^5 cells/cm^2; and placed onto six-well glass slides in an incubator for >3 days. Adherent cells (hepatocytes) were maintained in the medium.

For p-ASK1 staining, hepatocytes were fixed in 95% acetone for 30 seconds at room temperature and permeabilized in 0.1% Triton X-100 for 2 minutes at 4°C. Cells were then stained with a mouse monoclonal antibody to p-ASK1 (1:100; Wako Pure Chemical Co.) for 1 hour, washed with PBS, and reacted with Alexa Fluor Dyes (red stained)−conjugated goat anti-mouse IgG antibodies (Invitrogen). Isolated hepatocytes were observed and images immediately captured with a Nikon ECLIPSE E600 inverted fluorescence microscope (Nikon, Tokyo, Japan). We applied the HistoMouse *Plus* Kit (Invitrogen) to block endogenous mouse IgG.

Western Blot Analysis

Proteins (40 μg) isolated from BDL-injured livers of WT and *ASK1*$^{-/-}$ mice were separated by SDS-PAGE and transferred to Immun-Blot polyvinylidene difluoride membranes (Bio-Rad Laboratories, K.K., Tokyo, Japan) using a semidry blotter.[17,20,22−25,30] The blotted membranes were treated with 5% (w/v) skimmed milk in 10 mmol/L Tris, 150 mmol/L NaCl, and 0.2% (v/v) Tween-20 and incubated for 1 hour at room temperature with primary antibody. The following antibodies and dilutions were used: mouse monoclonal antibodies to phosphorylated JNK (p-JNK), JNK, phosphorylated p38 (p-p38), p38, proliferating cell nuclear antigen (PCNA) (1:200; Santa Cruz Biotechnology), or p-ASK1 (1:1000; Wako Pure Chemical Industries); goat polyclonal antibody to caspase-3 precursor (procaspase-3; 32 kDa) and caspase-3 subunit (active fragment; 11 kDa) (1:200; Santa Cruz Biotechnology)[6]; rabbit monoclonal antibody to ASK1 (1:2000; Abcam, Cambridge, UK); rabbit polyclonal antibodies to Bax (1:50; Santa Cruz Biotechnology); inducible nitric oxide synthase (iNOS: 1:200; BD Biosciences, San Jose, CA); or transforming growth factor β1 (activated TGF-β1: 25 kDa; 1:200; Santa Cruz Biotechnology) and 1:5000 dilution of anti−β-actin (Santa Cruz Biotechnology). The membranes were then incubated for 45 minutes at room temperature with a peroxidase-

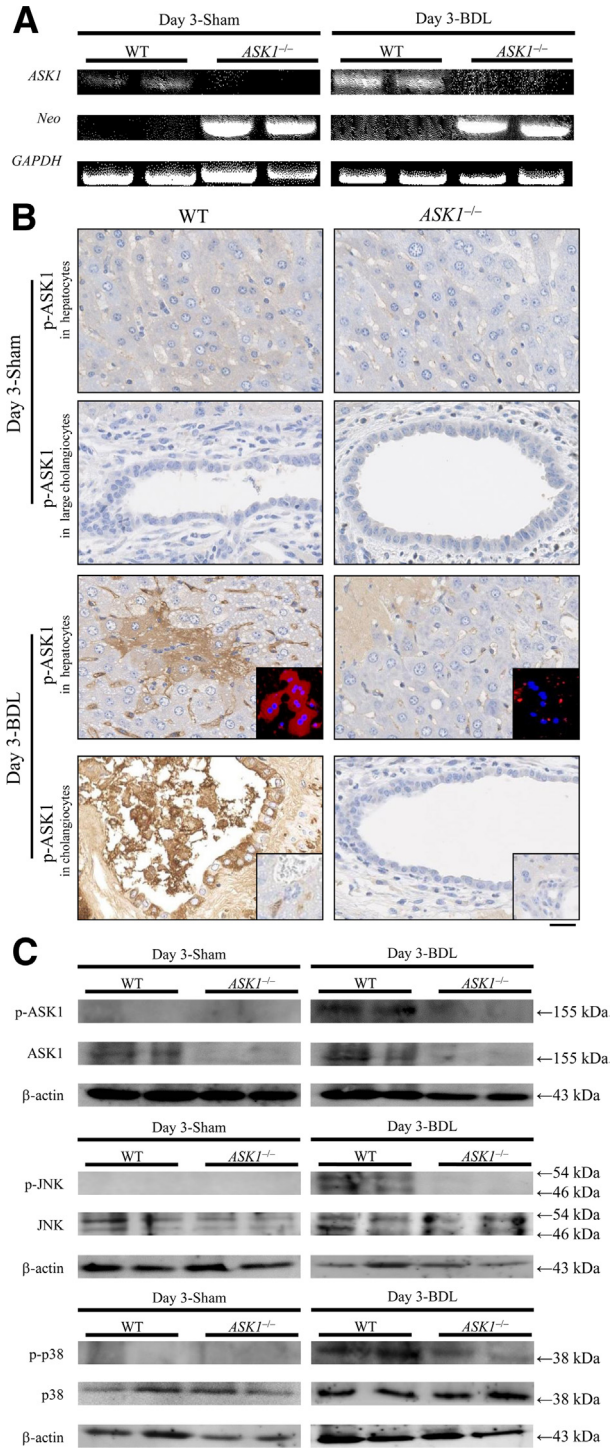

Figure 1 Analysis of ASK1 mRNA and protein expression in mice. **A:** RT-PCR of *ASK1* expression in livers of *ASK1*$^{-/-}$ and WT mice subjected to BDL surgery ($n = 10$ mice per group) and of controls (sham operated) ($n = 5$ mice per group). **B:** IHC of p-ASK1 at day 3 after BDL surgery ($n = 10$ mice per group). p-ASK1 is present in many hepatocytes and large but not small (**inset**) cholangiocytes throughout the livers of WT mice, but not in *ASK1*$^{-/-}$ mice, and sham-operated animals. Immunofluorescence staining of p-ASK1 (red stained) in cultured hepatocytes harvested from WT and *ASK1*$^{-/-}$ mice (**inset**). **C:** Western blot analysis of p-ASK1, ASK1, p-JNK, and p-p38 in day 3 BDL livers of *ASK1*$^{-/-}$ and WT mice ($n = 10$ mice per group) and control sham-operated mouse livers ($n = 5$ mice per group). Scale bar = 25 μm. Values were normalized for *GAPDH* expression (RT-PCR) (**A**) and for β-actin expression (Western blotting) (**C**).

conjugated secondary antibody and visualized using an ECL kit (GE Healthcare Bio-Science, Buckinghamshire, England, UK). Bands on Western blots were analyzed densitometrically using Scion Image software (version 4.0.2; Scion Corp., Frederick, MD).

ELISA for TNF-α and IL-1β

Levels of serum TNF-α and IL-1β in the BDL-injury model on day 3 were measured using an enzyme-linked immunosorbent assay (ELISA) kit according to the manufacturer's instructions (R&D Systems, Minneapolis, MN).[17,20,23–25]

Electron Microscopy

At day 14 after BDL surgery, injured livers from *ASK1*$^{-/-}$ and WT mice were fixed with 2.5% glutaraldehyde, and small specimens were cut (approximately 1 × 1 mm), including large cholangiocytes, and were immersed in 2% osmium tetroxide and dehydrated in ethanol. For transmission electron microscopy, dehydrated tissue specimens were embedded in epoxy resin. Silver-gold sections produced with a diamond knife were transferred to copper grids and stained with uranyl acetate for viewing on a transmission electron microscopy (JEM-1200EX; JEOL Ltd., Tokyo, Japan).

Statistical Analysis

Results are expressed as means ± SEM. Significant differences were analyzed using Student's *t*-test, Welch's *t*-test, or one-way analysis of variance where appropriate. In all cases when the analysis of variance method was used for nonparametric data, Tukey's multiple comparison *post hoc* test was used.[17,20,24,25] $P < 0.05$ was considered statistically significant.

Results

Expression of ASK1, p-ASK1, p-JNK, and p-p38 Is Absent or Decreased in Sham-Operated and/or BDL-Injured Livers of *ASK1*$^{-/-}$ Mice

Liver mRNA and protein expression levels of ASK1 and/or p-ASK1 were detected by RT-PCR and Western blotting, respectively. PCR clearly revealed no expression of *ASK1* in the livers of *ASK1*$^{-/-}$ mice with or without BDL on day 3 (Figure 1A). *ASK1* was only detected in WT mice, and its expression was significantly greater in BDL WT mice than in sham-operated WT mice (Figure 1A). In addition, immunofluorescence studies found that hepatocytes obtained from WT mice, but not those from *ASK1*$^{-/-}$ mice, expressed intracellular p-ASK1 (Figure 1B, inset). However, biochemical and morphologic (ratio of liver to body weight) studies revealed no differences in livers of *ASK1*$^{-/-}$ and WT mice under basal conditions (data not shown).

In mice subjected to day 3 BDL surgery, IHC (Figure 1B) and Western blotting (Figure 1C) confirmed that p-ASK1 and ASK1 protein was specifically expressed throughout the livers of WT mice (Figure 1, B and C), especially in cholangiocytes lining large but not small (Figure 1B, inset) bile ducts and hepatocytes around bile infarcts, but was not present in *ASK1*$^{-/-}$ mice and sham-operated animals (Figure 1B). Moreover, Western blotting analysis revealed that the expression of p-JNK and p-p38 in BDL-injured livers in *ASK1*$^{-/-}$ mice on day 3 was also significantly reduced compared with WT mice (Figure 1C).

Deletion of *ASK1* Suppresses Acute Cholestatic Liver Injury

The serum levels of ALT and AST were significantly increased in WT mice after 3 days of BDL compared with *ASK1*$^{-/-}$ mice (Figure 2A), indicative of more extensive hepatocyte necrosis and cell death (apoptosis). Similarly, total plasma and conjugated bilirubin (Figure 2B), plasma bile acid concentration (Figure 2C), hepatic levels of bile acids (Figure 2C), and cholesterol, especially very low-density lipoprotein (VLDL) and low-density lipoprotein (LDL) (data not shown), were significantly elevated in WT mice compared with *ASK1*$^{-/-}$ mice on day 3 after BDL surgery and control mice ($P < 0.05$ or $P < 0.001$, $P < 0.001$, and $P < 0.0001$, respectively). These *in vivo* bile acid levels <300 μmol/L (Figure 2C) in the BDL models are insufficient to not only directly cause liver cells death but also trigger inflammatory mediators formation, as described in the recent review paper.[32] Accumulation of conjugated bilirubin contributed to increased plasma bilirubin levels in both groups of mice with BDL (Figure 2B). The serum levels of alkaline phosphatase were markedly higher in the day 3 post−BDL surgery mice groups (2444 ± 491 U/L for the WT mice versus 2529 ± 322 U/L for the *ASK1*$^{-/-}$ mice) compared with sham-operated animals (165 ± 10 U/L for the WT mice versus 135 ± 21 U/L for the *ASK1*$^{-/-}$ mice); however, no significant difference was found between *ASK1*$^{-/-}$ and WT mice at day 3 after BDL surgery or controls, respectively (data not shown). According to the serum cholesterol profiles by high-performance liquid chromatography in mice at day 3 after BDL surgery, no significant difference was found in total cholesterol, high-density lipoprotein, or triglyceride levels between the two groups (data not shown). Both day 3 post−BDL surgery WT and *ASK1*$^{-/-}$ mice developed hypercholesterolemia and hypotriglyceridemia, with significantly increased levels of total cholesterol, VLDL, and LDL but decreased high-density lipoprotein cholesterol and triglyceride levels compared with control animals (data not shown). In addition, BDL resulted in increased urine bilirubin levels in WT and *ASK1*$^{-/-}$ mice. A similar pattern was observed without statistical significant between the

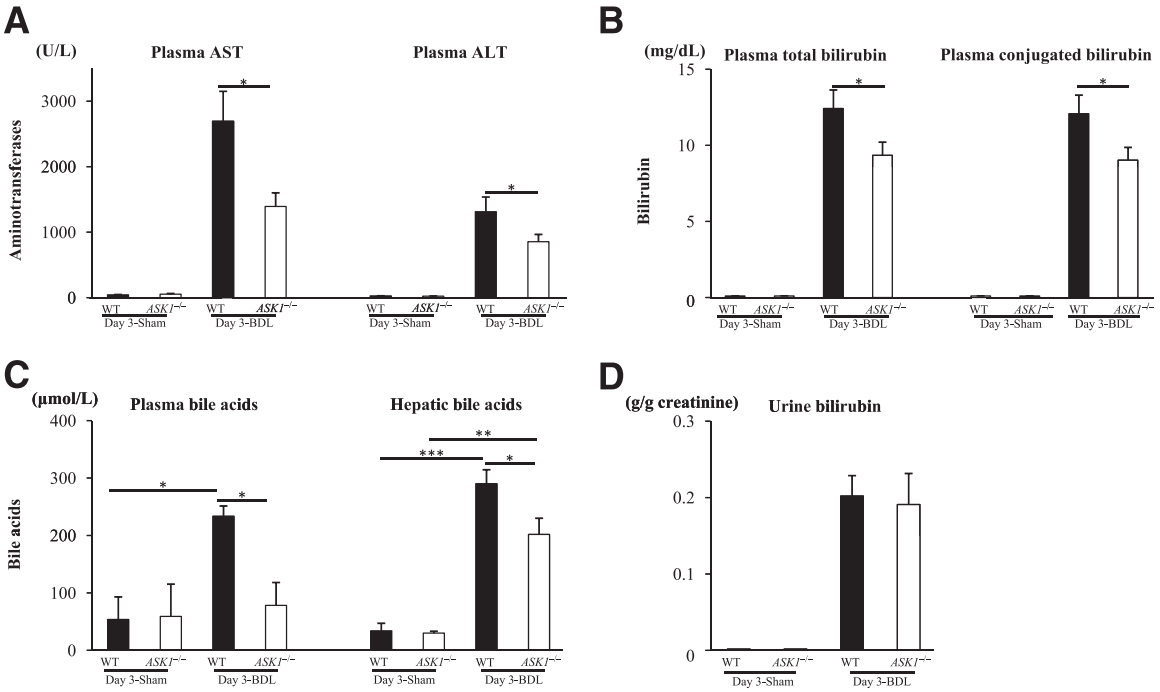

Figure 2 Effects of *ASK1* deletion on plasma aminotransferases, bilirubin, bile acid levels, and hepatic bile acid levels in the murine BDL model. **A:** Plasma AST and ALT levels in day 3 BDL WT and *ASK1*$^{-/-}$ mice ($n = 10$ mice per group) and control (sham-operated) mice ($n = 5$ mice per group) ($P < 0.0001$). **B:** Total and conjugated bilirubin levels in day 3 BDL WT and *ASK1*$^{-/-}$ mice ($n = 10$ mice per group) and control mice ($n = 5$ mice per group) ($P < 0.0001$). **C:** Levels of plasma and hepatic bile acids in day 3 BDL WT and *ASK1*$^{-/-}$ mice ($n = 10$ mice per group) and control mice ($n = 5$ mice per group). **D:** Urine bilirubin levels in day 3 BDL WT and *ASK1*$^{-/-}$ mice ($n = 10$ mice per group) and sham-operated animals ($n = 5$ mice per group). Values are means ± SEM. *$P < 0.05$, **$P < 0.001$, and ***$P < 0.0001$.

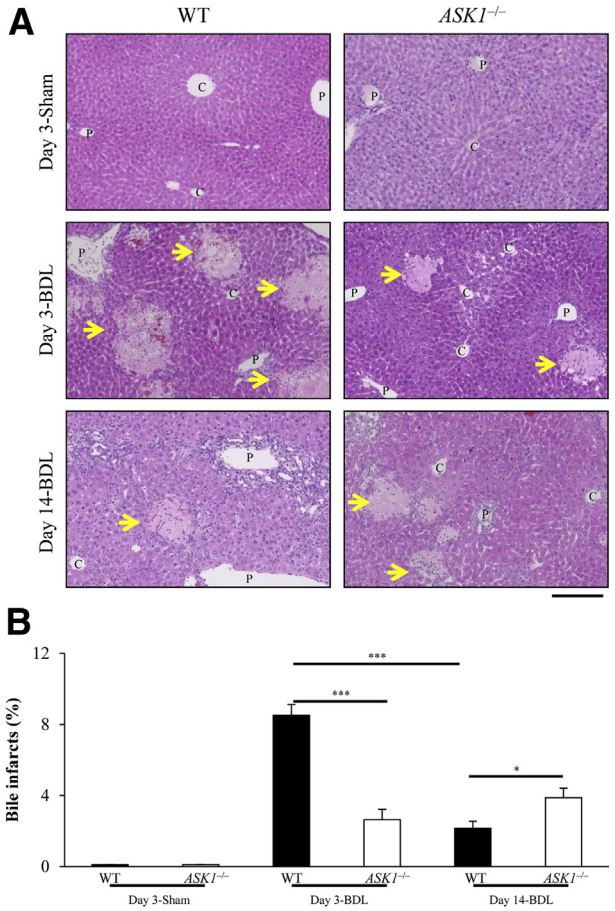

Figure 3 Histologic analysis of BDL-induced bile infarcts. **A:** Representative H&E-stained liver sections of WT and *ASK1*$^{-/-}$ mice 3 or 14 days after BDL surgery ($n = 10$ mice per group) are shown. Sham-operated livers from both groups of mice served as controls ($n = 5$ mice per group). **B:** Quantitative analysis of day 3 and day 14 post—BDL surgery *ASK1*$^{-/-}$ and WT mice (confluent necrotic foci of hepatocytes, indicated by **yellow arrows**). Injured livers in WT mice at day 14 after BDL surgery displayed a significantly smaller amount of infarcted areas, indicative of a faster repair process to acute cholestatic injury, compared with *ASK1*$^{-/-}$ mice. Values are means ± SEM. $^{**}P < 0.001$ and $^{***}P < 0.0001$. Scale bar = 200 μm. C, central vein; P, portal vein.

two groups of mice at day 3 after BDL surgery (Figure 2D). No statistical differences between genotypes were observed in sham-operated animals for any of the above parameters (Figure 2).

ASK1-Deficient Hepatocytes Are More Resistant to Acute Cholestatic Liver Injury but Delay Regeneration of BDL-Injured Livers

Corresponding to the above AST, ALT, or bilirubin data, the area of bile infarcts was significantly more extensive in WT mice than in *ASK1*$^{-/-}$ mice at day 3 after BDL surgery (8.51% ± 0.60% for WT mice versus 2.64% ± 0.58% for *ASK1*$^{-/-}$ mice; $P < 0.0001$) and control mice ($P < 0.0001$), respectively (Figure 3, A and B). Although liver histologic analysis in WT mice at day 14 after BDL surgery revealed significantly faster repair processes of acute cholestatic injury and smaller infarcted areas compared with *ASK1*$^{-/-}$ mice (2.15% ± 0.40% for WT mice versus 3.87% ± 0.54% for *ASK1*$^{-/-}$ mice; $P < 0.05$) (Figure 3, A and B). No significant difference was found between areas of bile infarcts at day 3 and 14 after BDL surgery in *ASK1*$^{-/-}$ mice, unlike in WT mice ($P < 0.0001$; Figure 3B). In addition, no difference was found in the ratios of liver to body weight at day 14 after BDL surgery between the two groups of mice (data not shown). However, significantly decreased cholestatic complications and mortality were observed in *ASK1*$^{-/-}$ mice 21 days after BDL surgery compared with WT mice (overall survival: 50.8% ± 5.6% for WT mice versus 77.8% ± 5.7% for *ASK1*$^{-/-}$ mice; $P < 0.0001$) (Supplemental Figure S1), whereas all control animals were free of complications and did not die during the study period.

Deletion of *ASK1* Does Not Affect Apoptotic Activity of Both Hepatocytes and Large Cholangiocytes after BDL

On the basis of morphologic analysis, such as cell shrinkage, chromatin condensation and margination, and formation of apoptotic bodies, the numbers of apoptotic liver cells 3 days after BDL surgery (0.04% ± 0.01% in WT mice versus 0.03% ± 0.01% in *ASK1*$^{-/-}$ mice of all hepatocytes; approximately 0.4 cells per 10 fields, respectively) (0.01% ± 0.01% in WT mice versus 0.01% ± 0.01% in *ASK1*$^{-/-}$ mice of all large cholangiocytes) were negligible (Supplemental Figure S2A) and not significantly increased compared with sham-operated controls (0.02% ± 0.02% of all hepatocytes) (0.01% ± 0.01% of all large cholangiocytes) in the H&E sections. Consistent with these findings, no significant differences were found in caspase-3 activities and caspase-3 processing (Supplemental Figure S2B) or Bax expression (data not shown) in Western blotting analysis between the respective groups (WT versus *ASK1*$^{-/-}$ mice and BDL versus sham surgery).

In striking contrast, the number of TUNEL^{+} interlobular hepatocytes around bile infarcts was significantly lower in *ASK1*$^{-/-}$ mice compared with WT mice (45.9 ± 2.4 per 10 fields in WT mice versus 39.6 ± 2.6 per 10 fields in *ASK1*$^{-/-}$ mice; $P < 0.05$) (data not shown). However, staining pattern was diffuse over the entire cell and did not remain confined to the nucleus as was seen in true apoptotic hepatocytes. Also, these oncotic hepatocytes were swollen with total nuclear fragmentation or cell lysis (ie, characteristics of necrosis). Therefore, no morphologically apoptotic characteristics were identified in most of the TUNEL^{+} hepatocytes. Furthermore, the number of TUNEL^{+} large cholangiocytes was significantly lower in *ASK1*$^{-/-}$ mice than in WT mice (7.6 ± 0.5 per 10 fields in WT mice versus 5.8 ± 0.4 per 10 fields in *ASK1*$^{-/-}$ mice; $P < 0.05$) (data not shown) but that of TUNEL^{+} small cholangiocytes was not (8.2 ± 0.7 per 10 fields in WT mice versus 8.1 ± 0.7 per 10 fields in *ASK1*$^{-/-}$ mice) (data not shown). Similarly, the morphologic characteristics of apoptosis were not noted in the TUNEL^{+}

cholangiocytes. In fact, double-immunofluorescence staining (data not shown) revealed that there were no apoptotic (green stained) $CK19^{+}$ large cholangiocytes (red stained). Livers of sham-operated control mice revealed no injury and no $TUNEL^{+}$ cells (data not shown).

Deletion of *ASK1* Represses Inflammatory Reactions in Interlobular and Portal Tracts after BDL Surgery

Gr-1 staining revealed significantly more decreasing numbers of accumulated neutrophils not only per injured interlobular areas in sinusoids or extravasated into the parenchymal tissue (total: 139.6 ± 4.1 per 10 fields in WT mice versus 105.8 ± 4.1 per 10 fields in $ASK1^{-/-}$ mice; $P < 0.0001$) (extravasated: 91.7 ± 2.6 per 10 fields in WT mice versus 61.5 ± 3.0 per 10 fields in $ASK1^{-/-}$ mice; $P < 0.0001$) (Figure 4A), but also per injured portal tracts (69.8 ± 3.6 per 10 fields in WT mice versus 61.5 ± 2.9 per 10 fields in $ASK1^{-/-}$ mice; $P < 0.05$) (Figure 4B) in $ASK1^{-/-}$ livers than in WT livers at day 3 after BDL surgery. Approximately 66% of these neutrophils were extravasated into the injured interlobular areas of WT livers, whereas 58% of those were located in the parenchyma in $ASK1^{-/-}$ livers ($P < 0.05$) (Figure 4A). Moreover, significantly extensive positive staining for chlorotyrosine protein adducts was recognized, especially in these interlobular areas around confluent bile infracts of day 3 post−BDL surgery WT livers, indicating that the extravasated neutrophils were cytotoxically active.[28] Only <5 neutrophils per 10 high-power fields were noted in sham-operated controls of both WT and $ASK1^{-/-}$ mice, respectively (data not shown), and no neutrophils were observed extravasated into the parenchyma.

Furthermore, IHC for CD3 revealed that modestly injured livers in $ASK1^{-/-}$ mice contained significantly fewer infiltrating T lymphocytes, especially around large bile ducts in the portal tracts, compared with WT mice at day 3 after BDL surgery (132.0 ± 10.1 per 10 fields in WT mice versus 100.2 ± 6.9 per 10 fields in $ASK1^{-/-}$ mice; $P < 0.05$)

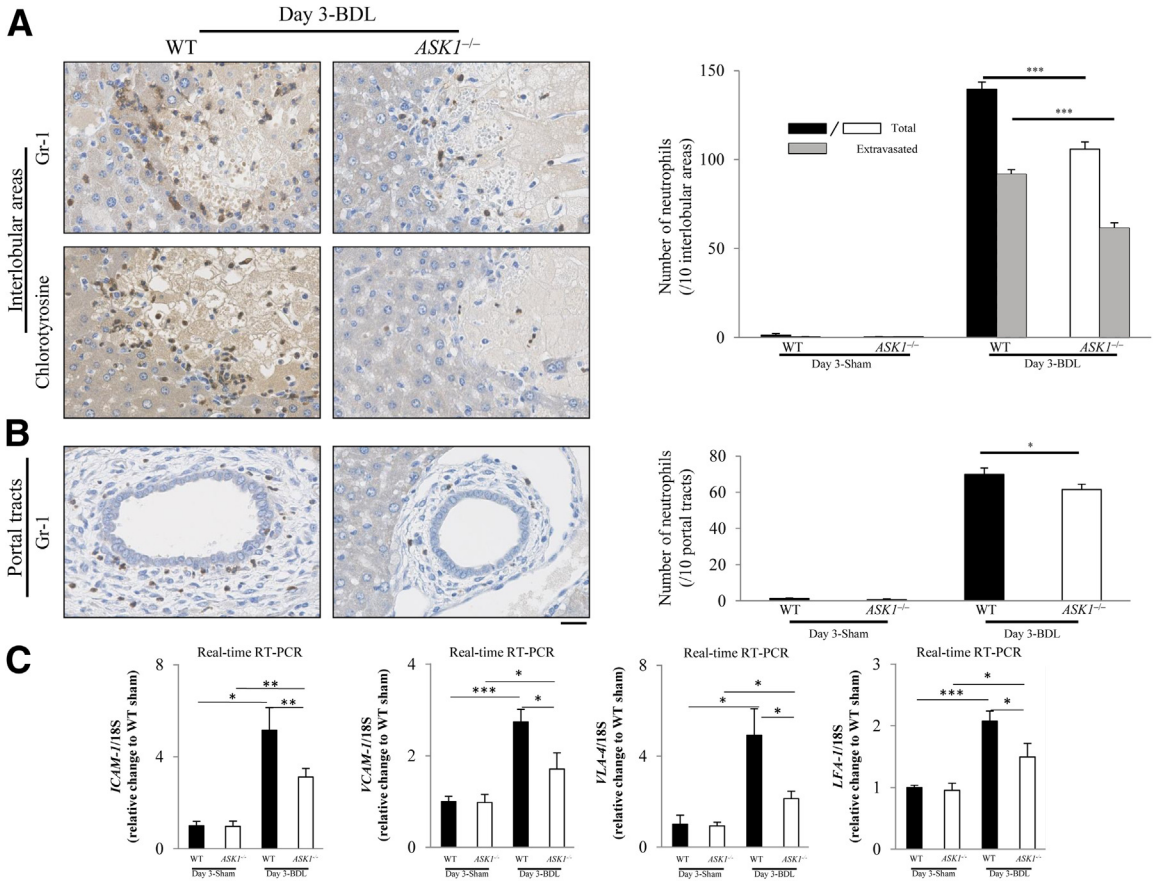

Figure 4 Analysis of infiltrating neutrophils and adhesion molecule expression in BDL-induced cholestatic livers of mice. **A:** IHC reveals the number of accumulated neutrophils per injured interlobular areas in sinusoids or extravasated into the parenchymal tissue of $ASK1^{-/-}$ and WT mice at day 3 after BDL surgery ($n = 10$ mice per group). Approximately 66% of these neutrophils were extravasated into the injured interlobular areas of WT livers, whereas significantly fewer (58%) of those were located in the parenchyma in $ASK1^{-/-}$ livers. Positivity for chlorotyrosine protein adducts was recognized, especially in these interlobular areas around confluent bile infarcts of day 3 post-BDL WT livers. Fewer than 5 neutrophils were noted in sham-operated controls of both WT and $ASK1^{-/-}$ mice ($n = 5$ mice per group), and no neutrophils extravasated into the parenchyma. **B:** There were few accumulated neutrophils per injured portal tracts in $ASK1^{-/-}$ and WT livers at day 3 after BDL surgery ($n = 10$ mice per group). **C:** Real-time RT-PCR of adhesion molecules, such as *ICAM-1*, *VCAM-1*, *VLA-4*, and *LFA-1*, in the injured livers of WT and $ASK1^{-/-}$ mice ($n = 10$ mice per group) at day 3 after BDL surgery and control mice ($n = 5$ mice per group). Values are means ± SEM and were normalized for 18s rRNA expression (real-time RT-PCR). $^{*}P < 0.05$, $^{**}P < 0.001$, and $^{***}P < 0.0001$. Scale bar = 25 μm.

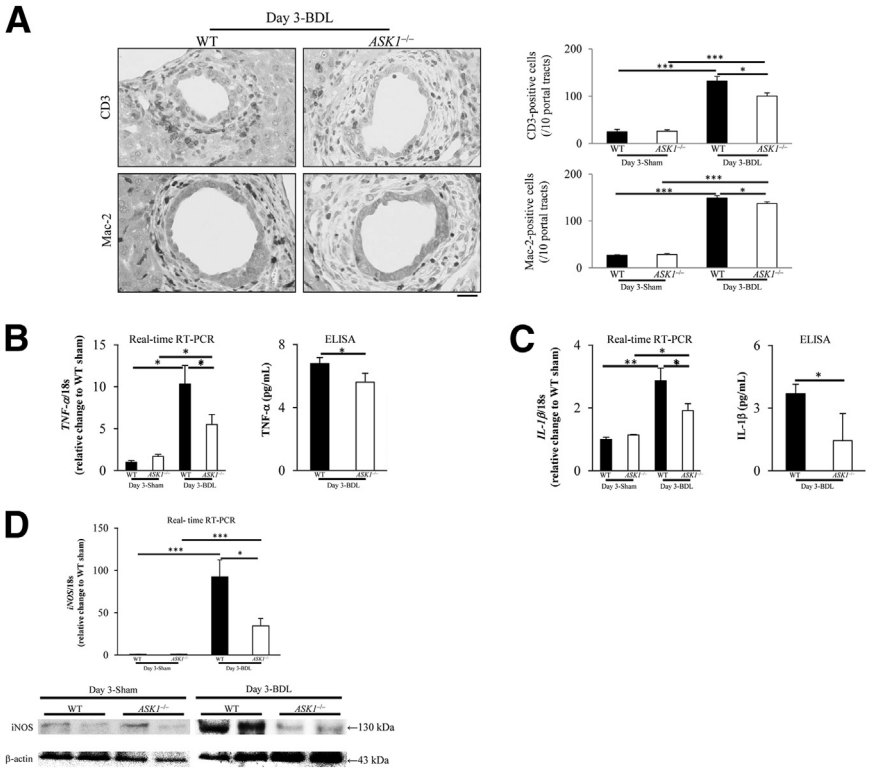

Figure 5 Analysis of infiltrating T lymphocytes or Kupffer cells and proinflammatory reactions in BDL-induced cholestatic livers of mice. **A:** IHC of infiltrating $CD3^+$ T lymphocytes and Mac-2^+ macrophages (Kupffer cells) around large bile ducts in the portal tracts of day 3 BDL WT mice compared with $ASK1^{-/-}$ mice ($n = 10$ mice per group) and control mice ($n = 5$ mice per group). **B and C:** Real-time RT-PCR of *TNF-α* (**B**) and *IL-1β* (**C**) expression in the injured livers of WT mice compared with $ASK1^{-/-}$ mice ($n = 10$ mice per group) and control mice ($n = 5$ mice per group). ELISA confirmed gene expression. **D:** Real-time RT-PCR and Western blotting of iNOS in day 3 post-BDL livers of WT and $ASK1^{-/-}$ mice ($n = 10$ mice per group) and control mice ($n = 5$ mice per group). Values are means ± SEM and were normalized for 18s rRNA expression (real-time RT-PCR) or β-actin expression (Western blotting), respectively. $^*P < 0.05$, $^{**}P < 0.001$, and $^{***}P < 0.0001$. Scale bar = 25 μm.

(Figure 5A). Mac-2 staining also revealed significantly fewer macrophages, including Kupffer cells, per injured portal tract in $ASK1^{-/-}$ livers than in WT livers (149.3 ± 4.9 per 10 fields in WT mice versus 137.5 ± 3.1 per 10 fields in $ASK1^{-/-}$ mice; $P < 0.05$) (Figure 5A). Neither CD3-positive T lymphocytes nor Mac-2–positive macrophages in interlobular areas around bile infarcts had significant differences in numbers between the two groups of day 3 post–BDL surgery mice (CD3: 143.7 ± 6.9 per 10 fields in WT mice versus 136.0 ± 7.6 per 10 fields in $ASK1^{-/-}$ mice) (Mac-2: 162.9 ± 2.8 per 10 fields in WT mice versus 160.1 ± 5.6 per 10 fields in $ASK1^{-/-}$ mice). Sham-operated animals had markedly fewer inflammatory cells (Figure 5A).

Real-time RT-PCR revealed that the expression levels of several adhesion molecules, such as intercellular adhesion molecule-1 (ICAM-1), vascular cell adhesion molecule-1 (VCAM-1), very late antigen-4 (VLA-4), and lymphocyte function-associated antigen-1 (LFA-1) (Figure 4C), and many proinflammatory signaling factors, such as TNF-α (Figure 5B), TNF receptor (TNFR) 2 (Supplemental Figure S3), IL-1β (Figure 5C), IL-1 receptor (IL-1R) 1, IL-6, nuclear factor-kappa B (NF-κB), interferon-γ (IFN-γ), Toll-like receptor 4 (TLR4) (Supplemental Figure S3), or iNOS (Figure 5D), were significantly down-regulated in the livers of day 3 post–BDL surgery $ASK1^{-/-}$ mice compared with WT and control mice ($P < 0.05$, $P < 0.001$, and $P < 0.0001$, respectively). Corresponding to these data, ELISA analysis found that serum TNF-α (Figure 5B) and IL-1β (Figure 5C) levels were significantly lower in $ASK1^{-/-}$ mice than in WT mice 3 days after BDL ligation (TNF-α: 6.79 ± 0.38 pg/mL in WT mice versus 5.61 ± 0.56 pg/mL in $ASK1^{-/-}$ mice, $P < 0.05$; IL-1β: 3.70 ± 0.45 pg/mL in WT mice versus 1.44 ± 1.30 pg/mL in $ASK1^{-/-}$ mice, $P < 0.05$). Moreover, the iNOS data were confirmed by Western blotting analysis (Figure 5D). No statistical differences between genotypes were observed in sham-operated animals for any the above parameters.

Deletion of *ASK1* Decreases Proliferating Activity of Hepatocytes and Large Cholangiocytes after BDL Surgery

It has been found that the proliferation of interlobular hepatocytes and portal and periportal (interface) cholangiocytes peaks during the first 5 days after BDL surgery.[32] At day 3 after BDL surgery, the numbers of hepatocytes around bile infarcts (48.2 ± 1.9 per 10 fields in WT mice versus 35.1 ± 0.8 per 10 fields in $ASK1^{-/-}$ mice; $P < 0.001$) (Figure 6A) and $Ki67^+$ large cholangiocytes (43.2 ± 1.4 per 10 fields in WT mice versus 35.1 ± 0.8 per 10 fields I $ASK1^{-/-}$ mice; $P < 0.001$) (Figure 6B) were significantly reduced in $ASK1^{-/-}$ mice compared with WT mice. In contrast, the number of $Ki67^+$ small cholangiocytes was relatively small and not statistically different between the two groups of mice (14.6 ± 1.0 per 10 fields in WT mice versus 14.3 ± 0.6 per 10 fields in $ASK1^{-/-}$ mice). Double-immunofluorescence staining (Figure 6B) confirmed that the proliferating cells (green stained) were partly $CK19^+$ large cholangiocytes (red stained). Similarly, the proliferation activity of $BrdU^+$ cholangiocytes in large bile ducts 3 days after BDL surgery was significantly different between the two groups of mice

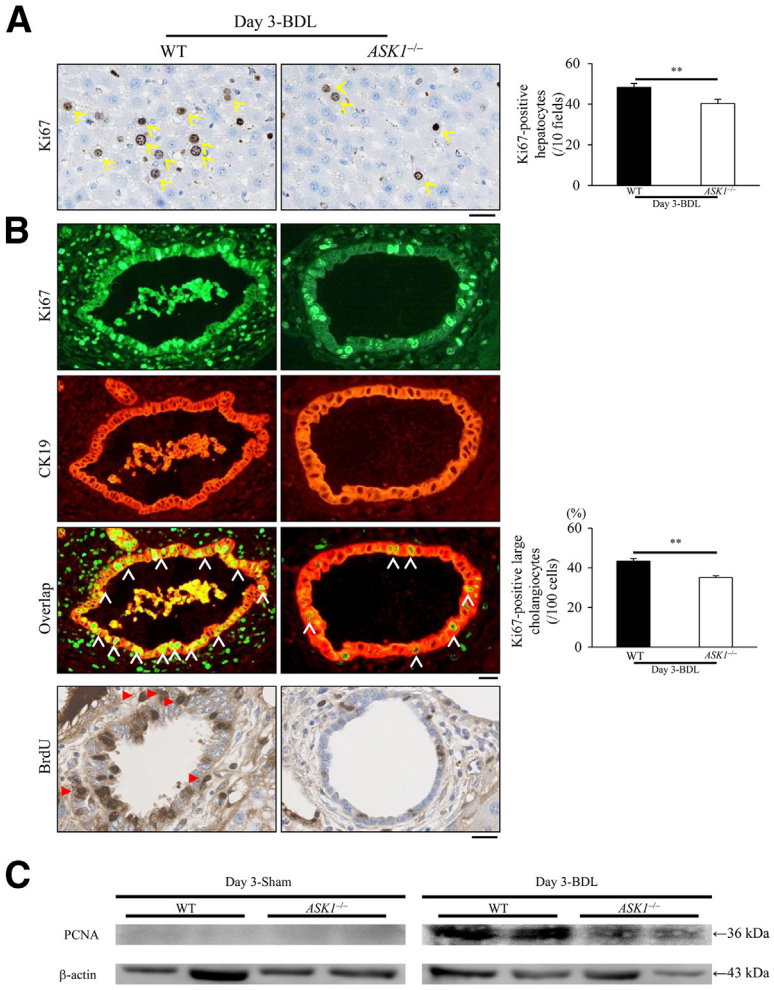

Figure 6 Analysis of proliferating liver cells in BDL-induced cholestasis. **A:** The number of Ki67$^+$ hepatocytes (indicated by **yellow arrowheads**) was significantly reduced in *ASK1*$^{-/-}$ compared with WT mice, measurements of Ki67$^+$ hepatocytes around bile infarcts, at day 3 after BDL surgery (n = 10 mice per group). **B:** Double-immunofluorescence staining revealed that proliferating cells in portal tracts (Ki67$^+$, green stained) were large cholangiocytes (CK19$^+$, red stained). The number of Ki67$^+$ and CK19$^+$ proliferating large cholangiocytes (**white arrowheads**) was markedly decreased in the portal tracts of day 3 post-BDL *ASK1*$^{-/-}$ mice than in WT mice (n = 10 mice per group). BrdU incorporation at day 3 after BDL surgery confirmed significant differences in proliferating large cholangiocytes between the two groups of mice. Interestingly, a substantial number of Ki67$^+$ or BrdU$^+$ oval to spindle myofibroblast-like cells are noted in the portal tracts of WT mice. Some BrdU-retaining spindle cells are located within large bile ducts (**red arrowheads**). **C:** Western blotting demonstrated that the hepatic expression of PCNA was significantly up-regulated in day 3 post-BDL WT and *ASK1*$^{-/-}$ mice (n = 10 mice per group) and control sham-operated mice (n = 5 mice per group). Values are means ± SEM (**A** and **B**) and were normalized for β-actin expression (Western blot analysis), respectively. $^{**}P < 0.001$. Scale bar = 25 μm.

(Figure 6B). Interestingly, a substantial number of Ki67$^+$ or BrdU$^+$ oval-to-spindle myofibroblast-like cells were also noted in portal tracts of WT mice at day 3 after BDL surgery (Figure 6B). In addition, some of the BrdU-retaining spindle cells were located within large bile ducts (Figure 6B).

Corresponding to the above histologic data, Western blotting analysis revealed that the expression of PCNA in modestly injured livers of *ASK1*$^{-/-}$ mice at day 3 after BDL surgery was significantly decreased compared with WT mice (Figure 6C). Sham-operated mice had no significant histologic or immunohistochemical differences between the two groups for any of the above parameters.

Deletion of *ASK1* Does Not Affect the Antioxidant State after BDL Surgery

Unexpectedly, serum TBARS levels were low in both *ASK1*$^{-/-}$ and WT mice at day 3 after BDL surgery and without statistical difference (0.87 ± 0.02 nmol MDA per milligram of LDL protein in WT mice versus 0.86 ± 0.04 nmol MDA per milligrams of LDL protein in *ASK1*$^{-/-}$ mice). Real-time RT-PCR revealed that the antioxidant family gene expressions of peroxiredoxin (*PRDX*) 1 to 6, catalase, or Cu, Zn-superoxide dismutase (*SOD*) 1 to 2 were not significantly different between the two groups (data not shown).

Deletion of *ASK1* Represses Activation of Peribiliary Fibrogenic Cells in or around Large Bile Ducts without Significant Proliferation after BDL Surgery

IBDM composed of CK19$^+$ large-to-small bile ducts was significantly decreased in *ASK1*$^{-/-}$ mice at day 14 after BDL surgery compared with WT mice (10.3% ± 0.6% in WT mice versus 8.8% ± 0.7% in *ASK1*$^{-/-}$ mice; $P < 0.05$) (Figure 7, A and B), indicating that deletion of *ASK1* could delay regenerative hyperplastic or proliferating responses of bile ducts against BDL injury. Similarly, IHC of day 14 BDL *ASK1*$^{-/-}$ mice livers revealed significantly lower specific and linear expression of α-SMA along the hyperplastic bile ductules and the hepatic sinusoids, in the portal and periportal tracts, compared with WT mice (5.9% ± 0.12% in WT mice versus 4.3% ± 0.1% in *ASK1*$^{-/-}$ mice; $P < 0.001$) (Figure 7, A and B). In mirror images of these sequential sections, α-SMA$^+$ but desmin$^-$

spindle to oval cells were easily detected in WT mice. These were consistent with the overt activation of peribiliary fibrogenic cells (ie, myofibroblasts), especially in WT mice, as previously described.[28] Similarly, real-time RT-PCR revealed that the expression levels of platelet-derived growth factor-BB (PDGF-BB) and PDGF receptor β (PDGFRB) (Supplemental Figure S3) were significantly down-regulated in the livers of day 3 BDL *ASK1*$^{-/-}$ mice compared with WT and control mice ($P < 0.05$ and $P < 0.0001$, respectively). Double-immunofluorescence staining (Figure 7C) revealed that a small number of hyperplastic CK19^{+} cholangiocytes (green-stained) concomitantly had a phenotype of α-SMA^{+} myofibroblasts (red-stained) in WT mice at day 14 after BDL surgery, which was rarely observed in *ASK1*$^{-/-}$ mice.

Ultrastructural Analysis of Portal Tracts in BDL-Injured Livers

Electron microscopy was performed to determine the phenotypes of *ASK1*-deficient stellate cells or large cholangiocytes in the portal and periportal tracts of day 14 BDL injured livers from *ASK1*$^{-/-}$ mice. Peribiliary fibrogenic cell phenotypes in the injured WT livers mainly had synthetic myofibroblast-like cells that contained significantly large amounts of cytoplasmic organelles, such as rough ER or lysosomes, compared with *ASK1*$^{-/-}$ mice (Supplemental Figure S4). ER and lysosome counts per peribiliary fibrogenic cell revealed statistically significant differences between the two groups of mice (7.6 ± 1.9 in WT mice versus 3.8 ± 0.9 in *ASK1*$^{-/-}$ mice; $P < 0.05$).

However, large cholangiocytes in day 14 BDL livers of *ASK1*$^{-/-}$ mice had a significantly higher density of microvilli for each cell, which characterized a phenotype of large or mature cholangiocytes[33] compared with WT mice (Supplemental Figure S4). Indeed, the morphologic features of large cholangiocytes in day 14 BDL injured livers of WT mice were not well preserved, displaying a significant decrease in density of microvilli per large cholangiocytes (10.5 ± 3.5 in WT mice versus 21.0 ± 1.6 in *ASK1*$^{-/-}$ mice; $P < 0.05$) (Supplemental Figure S4).

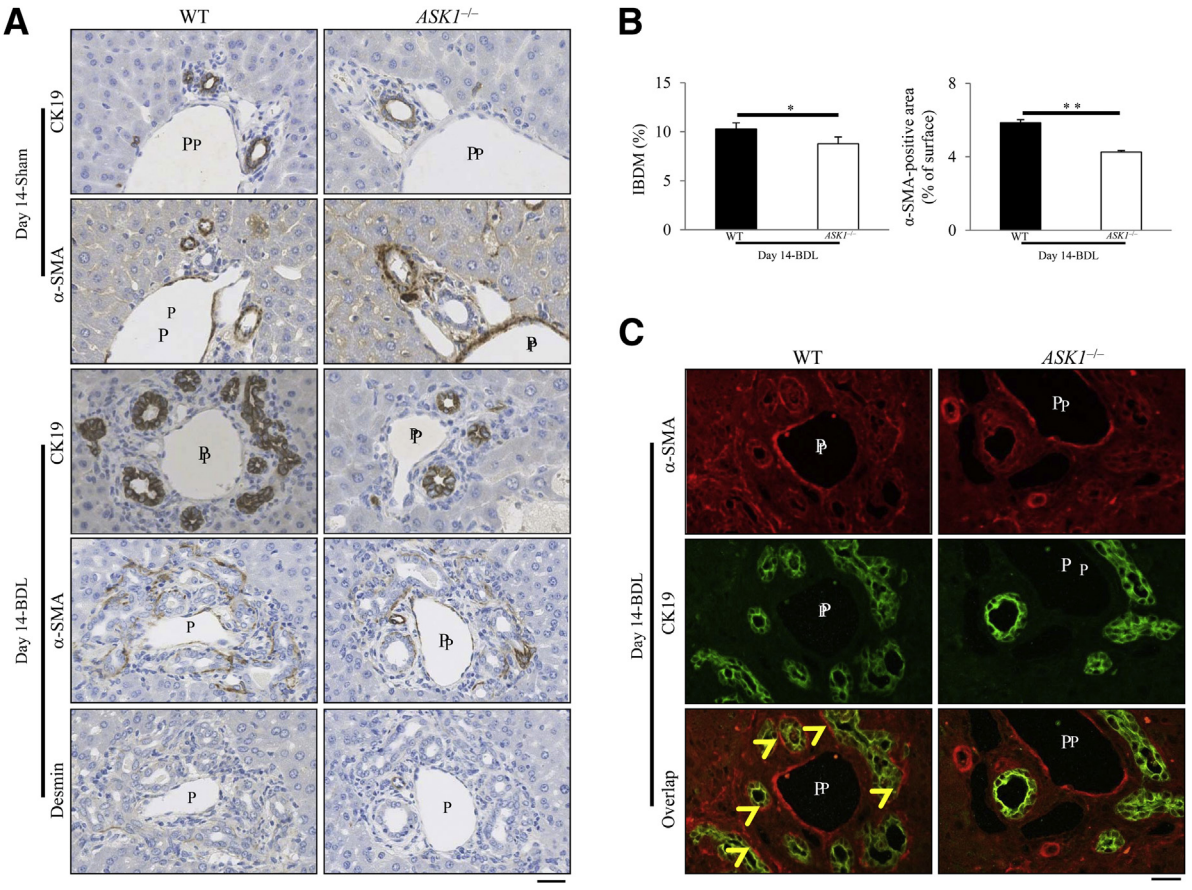

Figure 7 Measurements of IBDM and activated peribiliary fibrogenic cells in the BDL-induced cholestatic livers of mice. **A and B:** IHC For CK19, α-SMA, and desmin in portal and periportal tracts of day 14 BDL WT and *ASK1*$^{-/-}$ mice ($n = 10$ mice per group) and control sham-operated mice ($n = 5$ mice per group). **C:** Double immunofluorescence staining of hyperplastic CK19^{+} cholangiocytes (green-stained) and α-SMA^{+} activated peribiliary fibrogenic cells (red stained) in WT and *ASK1*$^{-/-}$ mice at day 14 after BDL surgery (**yellow arrowheads**). Values are means ± SEM. *$P < 0.05$ and **$P < 0.001$. Scale bar = 25 μm. P, portal vein.

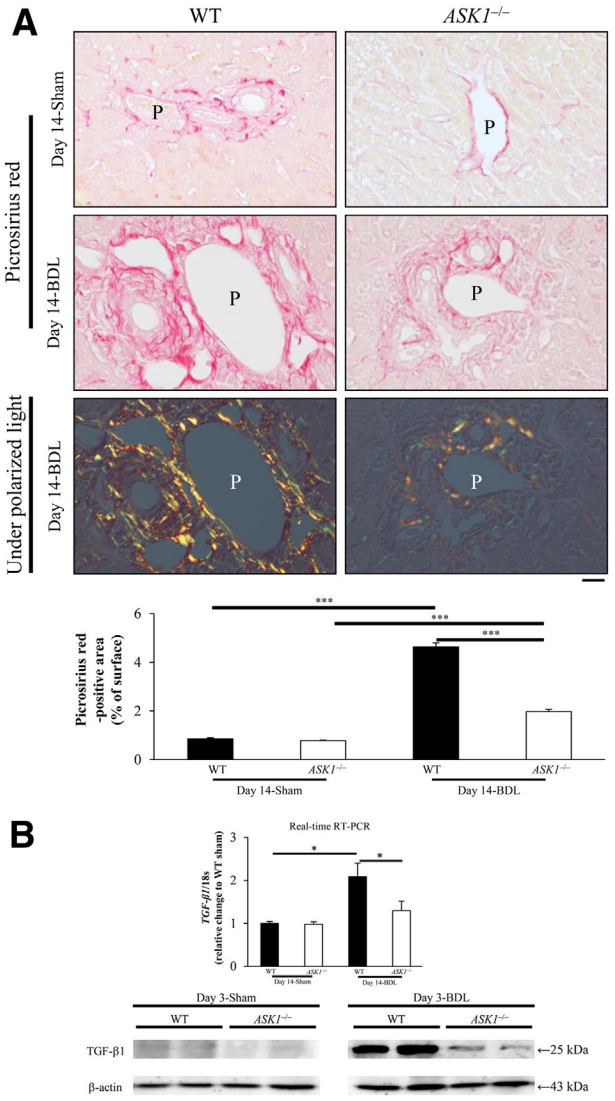

Figure 8 Analysis of peribiliary fibrosis or fibrogenesis in the BDL-induced cholestatic livers of mice. **A:** Picrosirius red staining reveals areas of peribiliary fibrosis or fibrogenesis in the cholestatic livers of WT and *ASK1*$^{-/-}$ mice at day 14 after BDL surgery ($n = 10$ mice per group) and sham-operated control mice ($n = 5$ mice per group). Under polarized light, the red-stained fibers expressed collagen type I, as shown by yellow birefringence. **B:** Real-time RT-PCR and Western blotting of activated TGF-β1 in day 14 post-BDL livers of WT and *ASK1*$^{-/-}$ mice ($n = 10$ mice per group) and control mice ($n = 5$ mice per group). Values are means ± SEM and were normalized for 18s rRNA expression (real-time RT-PCR) or β-actin expression (Western blotting), respectively. *$P < 0.05$ and ***$P < 0.0001$. Scale bar = 25 μm. P, portal vein.

Deletion of *ASK1* Suppresses Peribiliary Fibrosis or Fibrogenesis after BDL

Corresponding to the above IBDM or α-SMA IHC findings (Figure 7), picrosirius red staining revealed evidence of significantly greater peribiliary fibrosis in WT mice at day 14 after BDL surgery than in *ASK1*$^{-/-}$ mice (4.6% ± 0.2% in WT mice versus 2.0% ± 0.1% in *ASK1*$^{-/-}$ mice; $P < 0.0001$) and control mice ($P < 0.0001$) (Figure 8A). Similarly, Masson's trichrome staining in injured livers 14 days after BDL revealed significant differences between the two groups of mice (data not shown). Furthermore, real-time RT-PCR and Western blotting analyses revealed that the expression level of activated TGF-β1 (Figure 8B) was significantly down-regulated in the livers of day 14 BDL *ASK1*$^{-/-}$ mice compared with WT and control mice ($P < 0.05$).

No significant differences between genotypes were observed in sham-operated animals for any of the above parameters. Both groups of control mice had markedly less fibrosis and fibrogenesis compared with experimental groups (Figures 7A and 8A).

Microarray and Real-Time RT-PCR Analyses Reveal Variable Changes in Gene Expression Patterns, including Regulatory Genes of Bile Acid Synthesis, in BDL-Induced Cholestatic Models because of *ASK1* Deficiency

To identify new mechanisms involved in the suppression of liver necroinflammation and fibrosis or fibrogenesis observed in *ASK1*$^{-/-}$ mice, cDNA expression array analyses were performed comparing injured liver tissue samples obtained from *ASK1*$^{-/-}$ and *ASK1*$^{+/+}$ WT mice 3 days after BDL surgery. A total of 86 genes revealed a twofold change (58 up-regulated and 28 down-regulated genes) in *ASK1*$^{-/-}$ mice. The top up-regulated and down-regulated genes are listed in Supplementary Table S1. They include the up-regulation of the cytochrome P450 families, such as cholesterol 7α-hydroxylase (*CYP7A1*) or sterol 12α-hydroxylase (*CYP8B1*), components of bile acid metabolism,[34] and the down-regulation of IL-1 receptor type II (*IL-1R2*), a proinflammatory mediator, as well as *ASK1*. Real-time RT-PCR confirmed that the expression level of *CYP7A1* (Supplemental Figure S3) was significantly up-regulated in the livers of day 3 BDL *ASK1*$^{-/-}$ mice compared with WT and control mice ($P < 0.05$ or $P < 0.0001$, respectively). Conversely, the expression levels of small heterodimer partner (*SHP*), but not farnesoid X receptor (*FXR*) (Supplemental Figure S3), were significantly down-regulated in the modestly injured livers of day 3 post−BDL surgery *ASK1*$^{-/-}$ mice compared with WT mice ($P < 0.05$).

Discussion

The present study reveals, for the first time to our knowledge, a critical protective role of depleted ASK1 in a BDL injury−induced murine cholestasis model. Cholestasis-induced necroinflammation and fibrosis or fibrogenesis were significantly reduced, and the survival rate was increased in *ASK1*$^{-/-}$ mice having no expression of ASK1 compared with WT mice that expressed higher levels of

p-ASK1. *ASK1*$^{-/-}$ mice demonstrated potential anti-inflammatory profiles, especially in the acute phase of day 3 after BDL surgery, including manifestations of reduced bile infarcts, suppressed extensive inflammatory and proinflammatory reactions, lowered local (intrahepatic) and systemic (circulating) levels of bile acids, and decreased proliferation, but not apoptosis, in hepatocytes and large cholangiocytes. These effects also improved subsequent peribiliary fibrosis or fibrogenesis in *ASK1*-deleted mice with antifibrogenic profiles in the subacute (to chronic) phase of day 14 post-BDL injury. More recently, we found that *ASK1*$^{-/-}$ mice also had antiatherogenic (anti-inflammatory and/or antifibrogenic) features, especially in mechanical injury (carotid artery ligation)—induced vascular remodeling, manifesting as acute to subacute inflammatory disease (atherosclerosis).[20] In this context, *ASK1* deficiency would reveal significant protective effects against acute to subacute inflammatory injury. From other viewpoints, because *ASK1*$^{-/-}$ mice manifested as a delay of healing (ie, delayed repair process) in day 14 BDL livers, deletion of *ASK1* might partly display a detrimental profile in the subacute to chronic phase after BDL. Figure 9 summarizes the diverse roles of ASK1 in the murine BDL model. Furthermore, we proposed that BDL-induced oncotic necrosis and proliferation, but not apoptosis, are closely correlated with the severity of the inflammatory responses and that the pathogenic roles of ASK1-mediated necroinflammation and proliferation of not only hepatocytes but also large cholangiocytes are crucial in cholestasis-induced fibrosis or fibrogenesis.

After establishing the BDL model, we detected the specific expression of ASK1 and/or activated p-ASK1 in the injured livers of WT mice by RT-PCR, IHC, and Western blotting (Figure 1) but not in *ASK1*$^{-/-}$ mice. Interestingly, IHC (Figure 1B) revealed that there would be heterogeneity of p-ASK1 expression profiles in large versus small cholangiocytes, almost parallel to the severity of BDL-induced cholestatic injury, which might partly support the previous findings regarding the functional heterogeneities in large to small cholangiocytes.[12–14] The MAP3K family is likely stimulated by distinct mechanisms during the progression of cholestatic liver injury in response to various immune system mediators, such as TNF-α, IL-1β, or iNOS (Figure 6 and Supplemental Figure S3), and/or unknown ER and oxidative stressors. This subsequently increases the expression of activated downstream p-p38 and p-JNK. Indeed, the expression of these MAPK family members was significantly higher in WT livers than the modestly injured livers of *ASK1*$^{-/-}$ mice after BDL surgery (Figure 1C). However, only <0.1% of hepatocytes or large cholangiocytes were apoptotic even in both of the two groups at day 3 after BDL surgery, respectively (Supplemental Figure S2A), using morphologic criteria (ie, the gold standard to detect liver cells undergoing apoptosis after BDL, according to much of the recent data in the hepatology study).[5–9] Moreover, in particular, TUNEL^{+} hepatocytes had no apoptotic morphologic features because both of the nucleus and cytosol were stained, which is known to be characteristic of early necrosis.[35] Thus, these findings indicate that apoptosis plays little role in BDL-induced cholestasis and that *ASK1*$^{-/-}$ mice could be a good model for determining the net effects of blocked ASK1 signaling pathway in cholestatic necroinflammation and fibrosis.

Our data are in agreement with various previous observations from several other laboratories. Hepatic inflammation that involves the accumulation and recruitment of neutrophils, Kupffer cells, or T lymphocytes (Figures 4 and 5), all of which are cellular components of the innate to adapted immune system, plays a critical role in contributing to a large fraction of oncotic necrosis and subsequent fibrosis or fibrogenesis during murine BDL models.[6,8,9,28] Moreover, it is accompanied by not only the stimulation of various adhesion molecules and proinflammatory cascades[6,8,9,28] but also significant up-regulation of TGF-β1.[8,9] Interestingly, iNOS was markedly expressed in injured liver cells of WT mice (Figure 5D) in response to hepatic activation through various inflammatory and proinflammatory cytokines, including TNF-α or IL-1β (Figure 5, B and C and Supplemental Figure S3), and stimulated p38 MAPK-mediated signaling (Figure 1C), similar to mouse astrocytes or bovine chondrocytes, as previously described.[36,37]

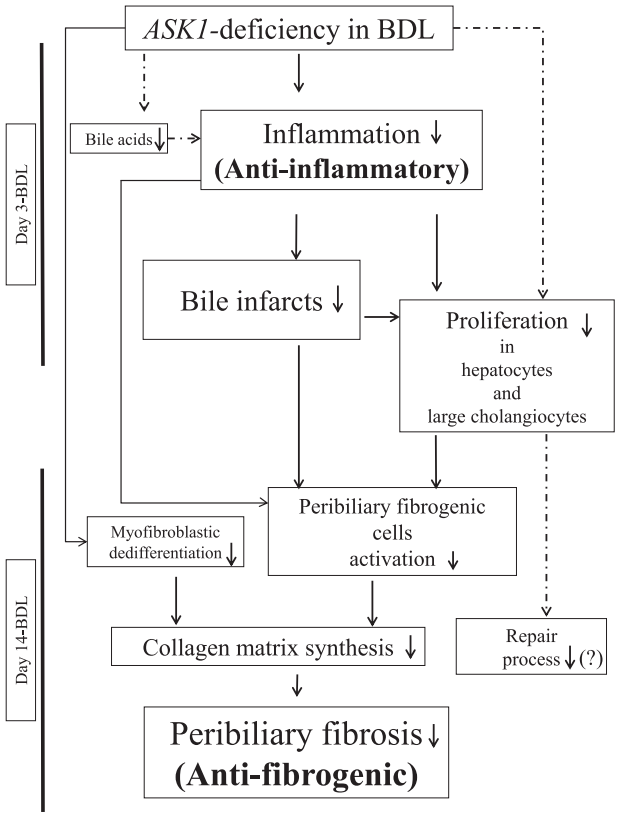

Figure 9 The critical roles of ASK1 in BDL-induced cholestasis. This diagram depicts the diverse, key roles of ASK1 in the current BDL-induced murine cholestatic model.

Furthermore, corresponding to Yes-associated protein–deficient mice demonstrating suppressed proliferation of large cholangiocytes in day 5 BDL livers with following increased bile infarcts at day 15 after BDL surgery,[38] *ASK1*$^{-/-}$ mice had significantly fewer proliferating hepatocytes and large cholangiocytes and reduced PCNA expression at day 3 after BDL surgery (Figure 5), together with greater necrotic foci in day 14 BDL livers (Figure 3). On the one hand, on the basis of a vast amount of results, this is just a consequence of reduced early-phase liver injury (ie, necroinflammation) in *ASK1*$^{-/-}$ mice rather than ASK1 directly affecting proliferation. On the other hand, because ASK1 is situated in an important upstream position for many signal transduction pathways, *ASK1* deficiency suppresses many signals required for not only inflammation but also cell survival or proliferation.[15,17,20] Therefore, the ASK1 pathway might have a close relationship with PCNA-induced proliferation signaling in liver cells, supported by the reported data that inhibition of the JNK pathway induces diminished proliferative responses to partial hepatectomy together with decreased PCNA expression.[39] Nevertheless, further studies are needed to clarify those issues because identifying promising key factors and pathways related to the MAP3K family member, ASK1, would help control hepatic responses against cholestasis-induced liver injury.

The present pathologic or molecular findings should be remarkable for other reasons. First, double-immunofluorescence staining with CK19 and α-SMA indicated a small number of hyperplastic cells (within IBDM) having phenotypes of both cholangiocytes and peribiliary fibrogenic cells, especially in WT mice at day 14 after BDL surgery, but which were absent or very rare in *ASK1*$^{-/-}$ mice (Figure 7C). The double-stained immature and precursor-like cells should play a key role in the repair process of injured cholangiocytes during cholestasis because hyperplastic or proliferating cholangiocytes could originate from pleiotropic hepatic stem or progenitor cells.[40] Second, ultrastructural analysis confirmed that hyperplastic large cholangiocytes in WT mice at day 14 after BDL surgery manifested as a phenotype of immature cholangiocytes (ie, differentiation of small into large cholangiocytes).[12–14] These cholangiocytes had significantly fewer microvilli, compared with *ASK1*$^{-/-}$ mice, and displayed overtly well-preserved morphologic features (Supplemental Figure S4). Furthermore, electron microscopy revealed that peribiliary fibrogenic cells from WT mice also had a dedifferentiated (immature) synthetic myofibroblast-like phenotype, containing a significantly larger number of cell organelles (Supplemental Figure S4). This is similar to the migrating intimal smooth muscle cells in injured arteries, as previously described by us.[20] The activated p38 MAPK pathway plays a crucial role in myofibroblastic dedifferentiation of not only smooth muscle cells[20,41] but also possibly peribiliary fibrogenic cells. These features are in line with significantly increased collagen production in day 14 BDL livers from WT mice (Figure 8). Third, cDNA expression array analyses revealed the significant up-regulation of cytochrome P450 families in *ASK1*$^{-/-}$ mice livers at day 3 after BDL surgery, including *CYP7A1* or *CYP8B1*, which are key regulated enzymes in bile acid synthesis (Supplemental Table S1).[42] Because significantly lower levels of bile acids in the *ASK1*$^{-/-}$ livers (Figure 2C) possibly activate *FXR* less and subsequently up-regulate *SHP* less (Supplemental Figure S3), involving the inhibition of SHP-mediated *CYP7A1* repression,[34] these data might be consistent with the potential anticholestatic profile, especially in the acute phase of the BDL model.

In conclusion, on the basis of our collected data, we postulate that *ASK1* deficiency plays critical roles in ameliorating cholestatic liver injury together with i) decreased accumulation and recruitment of various inflammatory cells into interlobular and portal areas accompanied by down-regulated expression of various adhesion molecules and proinflammatory mediators, ii) reduced hepatocellular necrosis (bile infarcts), iii) suppressed proliferation of hepatocytes and large cholangiocytes, iv) inactivation and rare myofibroblastic dedifferentiation in peribiliary fibrogenic cells, and v) repressed synthesis of collagen-rich extracellular matrix by the above mechanisms, as summarized in Figure 9. Hence, we can conclude that depletion of ASK1 prevents the development of acute necroinflammation and subsequent peribiliary fibrosis or fibrogenesis, suppressing aberrant regenerative (proliferating) responses and exerting beneficial effects in BDL injury–induced cholestasis. All these features indicate that a specific ASK1 pathway blocker could offer a therapeutic strategy against the progression of human cholestatic liver disease.

Acknowledgments

We thank Hiroko Isagai, Hana Nishimura, and Naoko Une for their expert technical assistance.

Supplemental Data

Supplemental material for this article can be found at *http://dx.doi.org/10.1016/j.ajpath.2013.11.030*.

References

1. Miyoshi H, Rust C, Roberts PJ, Burgart LJ, Gores GJ: Hepatocyte apoptosis after bile duct ligation in the mouse involves Fas. Gastroenterology 1999, 117:669–677
2. Canbay A, Higuchi H, Bronk SF, Taniai M, Sebo TJ, Gores GJ: Fas enhances fibrogenesis in the bile duct ligated mouse: a link between apoptosis and fibrosis. Gastroenterology 2002, 123:1323–1330
3. Yoon JH, Gores GJ: Death receptor-mediated apoptosis and the liver. J Hepatol 2002, 37:400–410
4. Canbay A, Taimr P, Torok N, Higuchi H, Friedman S, Gores GJ: Apoptotic body engulfment by a human stellate cell line is profibrogenic. Lab Invest 2003, 83:655–663
5. Schoemaker MH, Gommans WM, Conde de la Rosa L, Homan M, Klok P, Trautwein C, van Goor H, Poelstra K, Haisma HJ, Jansen PL, Moshage H: Resistance of rat hepatocytes against bile acid-induced apoptosis in cholestatic liver injury is due to nuclear factor-kappa B activation. J Hepatol 2003, 39:153–161

6. Gujral JS, Liu J, Farhood A, Jaeschke H: Reduced oncotic necrosis in Fas receptor-deficient C57BL/6J-lpr mice after bile duct ligation. Hepatology 2004, 40:998−1007
7. Fickert P, Trauner M, Fuchsbichler A, Zollner G, Wagner M, Marschall HU, Zatloukal K, Denk H: Oncosis represents the main type of cell death in mouse models of cholestasis. J Hepatol 2005, 42: 378−385
8. Nalapareddy PD, Schüngel S, Hong JY, Manns MP, Jaeschke H, Vogel A: The BH3-only protein bid does not mediate death-receptor-induced liver injury in obstructive cholestasis. Am J Pathol 2009, 175: 1077−1085
9. Mitchell C, Mahrouf-Yorgov M, Mayeuf A, Robin MA, Mansouri A, Fromenty B, Gilgenkrantz H: Overexpression of Bcl-2 in hepatocytes protects against injury but does not attenuate fibrosis in a mouse model of chronic cholestatic liver disease. Lab Invest 2011, 91:273−282
10. Lazaridis KN, Strazzabosco M, Larusso NF: The cholangiopathies: disorders of biliary epithelia. Gastroenterology 2004, 127:1565−1577
11. Yahagi K, Ishii M, Kobayashi K, Ueno Y, Mano Y, Niitsuma H, Igarashi T, Toyota T: Primary culture of cholangiocytes from normal mouse liver. In Vitro Cell Dev Biol Anim 1998, 34:512−514
12. Alpini G, Glaser S, Ueno Y, Pham L, Podila PV, Caligiuri A, LeSage G, LaRusso NF: Heterogeneity of the proliferative capacity of rat cholangiocytes after bile duct ligation. Am J Physiol Gastrointest Liver Physiol 1998, 274:G767−G775
13. LeSage G, Glaser S, Marucci L, Benedetti A, Phinizy JL, Rodgers R, Caligiuri A, Papa E, Tretjak Z, Jezequel AM, Holcomb LA, Alpini G: Acute carbon tetrachloride feeding induces damage of large but not small cholangiocytes from BDL rat liver. Am J Physiol Gastrointest Liver Physiol 1999, 276:G1289−G1301
14. Glaser S, Gaudio E, Rao A, Pierce LM, Onori P, Franchitto A, Francis HL, Dostal DE, Venter JK, DeMorrow S, Mancinelli R, Carpino G, Alvaro D, Kopriva SE, Savage JM, Alpini G: Morphological and functional heterogeneity of the mouse intrahepatic biliary epithelium. Lab Invest 2009, 89:456−469
15. Ichijo H, Nishida E, Irie K, Digike PT, Saitoh M, Moriguchi T, Takagi M, Matsumoto K, Miyazono K, Gotoh Y: Induction of apoptosis by ASK1, mammalian MAPKKK that activates SAPK/JNK and p38 signaling pathways. Science 1997, 275:90−94
16. Tobiume K, Matsuzawa A, Takahashi T, Nishitoh H, Morita K, Takeda K, Minowa O, Miyazono K, Noda T, Ichijo H: ASK1 is required for sustained activations of JNK/p38 MAP kinases and apoptosis. EMBO Rep 2001, 2:222−228
17. Yamada S, Ding Y, Tanimoto A, Wang KY, Guo X, Li Z, Tasaki T, Nabesima A, Murata Y, Shimajiri S, Kohno K, Ichijo H, Sasaguri Y: Apoptosis signal-regulating kinase 1 deficiency accelerates hyperlipidemia-induced atheromatous plaques via suppression of macrophage apoptosis. Arterioscler Thromb Vasc Biol 2011, 31: 1555−1564
18. Watanabe T, Otsu K, Takeda T, Yamaguchi O, Hikoso S, Kashiwase K, Higuchi Y, Taniike M, Nakai A, Matsumura Y, Nishida K, Ichijo H, Hori M: Apoptosis signal-regulating kinase 1 is involved not only in apoptosis but also in non-apoptotic cardiomyocyte death. Biochem Biophys Res Commun 2005, 333: 562−567
19. Liu Q, Sargent MA, York AJ, Molkentin JD: ASK1 regulates cardiomyocyte death but not hypertrophy in transgenic mice. Circ Res 2009, 105:1110−1117
20. Tasaki T, Yamada S, Guo X, Tanimoto A, Wang KY, Nabeshima A, Kitada S, Noguchi H, Kimura S, Shimajiri S, Kohno K, Ichijo H, Sasaguri Y: Apoptosis signal-regulating kinase 1 deficiency attenuates vascular injury-induced neointimal hyperplasia by suppressing apoptosis in smooth muscle cells. Am J Pathol 2013, 182:597−609
21. Makena PS, Gorantla VK, Ghosh MC, Bezawada L, Kandasamy K, Balazs L, Luellen CL, Thompson KE, Parthasarathi K, Ichijo H, Waters CM, Sinclair SE: Deletion of apoptosis signal-regulating kinase-1 prevents ventilator-induced lung injury in mice. Am J Respir Cell Mol Biol 2012, 46:461−469
22. Yamada S, Wang KY, Tanimoto A, Fan J, Shimajiri S, Kitajima S, Morimoto M, Tsutui M, Watanabe T, Yasumoto K, Sasaguri Y: Matrix metalloproteinase 12 accelerates the initiation of atherosclerosis and stimulates the progression of fatty streaks to fibrous plaques in transgenic rabbits. Am J Pathol 2008, 172:1419−1429
23. Ding Y, Yamada S, Wang KY, Shimajiri S, Guo X, Tanimoto A, Murata Y, Kitajima S, Watanabe T, Izumi H, Kohno K, Sasaguri Y: Overexpression of peroxiredoxin 4 protects against high-dose streptozotocin-induced diabetes by suppressing oxidative stress and cytokines in transgenic mice. Antioxid Redox Signal 2010, 13: 1477−1490
24. Guo X, Yamada S, Tanimoto A, Ding Y, Wang KY, Shimajiri S, Murata Y, Kimura S, Tasaki T, Nabeshima A, Watanabe T, Kohno K, Sasaguri Y: Overexpression of peroxiredoxin 4 attenuates atherosclerosis in apolipoprotein E knockout mice. Antioxid Redox Signal 2012, 17:1362−1375
25. Nabeshima A, Yamada S, Guo X, Tanimoto A, Wang KY, Shimajiri S, Kimura S, Tasaki T, Noguchi H, Kitada S, Watanabe T, Fujii J, Kohno K, Sasaguri Y: Peroxiredoxin 4 protects against nonalcoholic steatohepatitis and type 2 diabetes in a nongenetic mouse model. Antioxid Redox Signal 2013, 19:1983−1998
26. Mancinelli R, Franchitto A, Gaudio E, Onori P, Glaser S, Francis H, Venter J, Demorrow S, Carpino G, Kopriva S, White M, Fava G, Alvaro D, Alpini G: After damage of large bile ducts by gamma-aminobutyric acid, small ducts replenish the biliary tree by amplification of calcium-dependent signaling and de novo acquisition of large cholangiocyte phenotypes. Am J Pathol 2010, 176: 1790−1800
27. Horlad H, Fujiwara Y, Takemura K, Ohnishi K, Ikeda T, Tsukamoto H, Mizuta H, Nishimura Y, Takeya M, Komohara Y: Corosolic acid impairs tumor development and lung metastasis by inhibiting the immunosuppressive activity of myeloid-derived suppressor cells. Mol Nutr Food Res 2013, 57:1046−1054
28. Gujral JS, Farhood A, Bajt ML, Jaeschke H: Neutrophils aggravate acute liver injury during obstructive cholestasis in bile duct-ligated mice. Hepatology 2003, 38:355−363
29. Kinnman N, Francoz C, Barbu V, Wendum D, Rey C, Hultcrantz R, Poupon R, Housset C: The myofibroblastic conversion of peribiliary fibrogenic cells distinct from hepatic stellate cells is stimulated by platelet-derived growth factor during liver fibrogenesis. Lab Invest 2003, 83:163−173
30. Wang KY, Tanimoto A, Yamada S, Guo X, Ding Y, Watanabe T, Watanabe T, Kohno K, Hirano K, Tsukada H, Sasaguri Y: Histamine regulation in glucose and lipid metabolism via histamine receptors: model for nonalcoholic steatohepatitis in mice. Am J Pathol 2010, 177: 713−723
31. Yasuniwa Y, Izumi H, Wang KY, Shimajiri S, Sasaguri Y, Kawai K, Kasai H, Shimada T, Miyake K, Kashiwagi E, Hirano G, Kidani A, Akiyama M, Han B, Wu Y, Ieiri I: Circadian disruption accelerates tumor growth and angio/stromagenesis through a Wnt signaling pathway. PLoS One 2010, 5:e15330
32. Woolbright BL, Jaeschke H: Novel insight into mechanisms of cholestatic liver injury. World J Gastroenterol 2012, 18:4985−4993
33. Gradilone SA, Masyuk AI, Splinter PL, Banales JM, Huang BQ, Tietz PS, Masyuk TV, Larusso NF: Cholangiocyte cilia express TRPV4 and detect changes in luminal tonicity inducing bicarbonate secretion. Proc Natl Acad Sci U S A 2007, 104:19138−19143
34. Georgiev P, Jochum W, Heinrich S, Jang JH, Nocito A, Dahm F, Clavien PA: Characterization of time-related changes after experimental bile duct ligation. Br J Surg 2008, 95:646−656
35. Grasl-Kraupp B, Ruttkay-Nedecky B, Koudelka H, Bukowska K, Bursch W, Schulte-Hermann R: In situ detection of fragmented DNA (TUNEL assay) fails to discriminate among apoptosis, necrosis, and autolytic cell death: a cautionary note. Hepatology 1995, 21: 1465−1468

36. Da Silva J, Pierrat B, Mary JL, Lesslauer W: Blockade of p38 mitogen-activated protein kinase pathway inhibits inducible nitric-oxide synthase expression in mouse astrocytes. J Biol Chem 1997, 272: 28373–28380
37. Badger AM, Cook MN, Lark MW, Newman-Tarr TM, Swift BA, Nelson AH, Barone FC, Kumar S: SB 203580 inhibits p38 mitogen-activated protein kinase, nitric oxide production, and inducible nitric oxide synthase in bovine cartilage-derived chondrocytes. J Immunol 1998, 161:467–473
38. Bai H, Zhang N, Xu Y, Chen Q, Khan M, Potter JJ, Nayar SK, Cornish T, Alpini G, Bronk S, Pan D, Anders RA: Yes-associated protein regulates the hepatic response after bile duct ligation. Hepatology 2012, 56:1097–1107
39. Schwabe RF, Bradham CA, Uehara T, Hatano E, Bennett BL, Schoonhoven R, Brenner DA: c-Jun-N-terminal kinase drives cyclin D1 expression and proliferation during liver regeneration. Hepatology 2003, 37:824–832
40. Cantz T, Manns MP, Ott M: Stem cells in liver regeneration and therapy. Cell Tissue Res 2008, 331:271–282
41. Hayashi K, Takahashi M, Kimura K, Nishida W, Saga H, Sobue K: Changes in the balance of phosphoinositide 3-kinase/protein kinase B (Akt) and the mitogen-activated protein kinases (ERK/p38 MAPK) determine a phenotype of visceral and vascular smooth muscle cells. J Cell Biol 1999, 145:727–740
42. Lefebvre P, Cariou B, Lien F, Kuipers F, Staels B: Role of bile acids and bile acid receptors in metabolic regulation. Physiol Rev 2009, 89:147–191